LETTERS
https://doi.org/10.1038/s41556-020-0473-4

nature cell biology

Check for updates

Hrd1 forms the retrotranslocation pore regulated by auto-ubiquitination and binding of misfolded proteins

Vedran Vasic[1,4], Niels Denkert[1,2,4], Claudia C. Schmidt[1], Dietmar Riedel[3], Alexander Stein[1]✉ and Michael Meinecke[2]✉

During endoplasmic-reticulum-associated protein degradation (ERAD), misfolded proteins are polyubiquitinated, extracted from the ER membrane and degraded by the proteasome[1–4]. In a process called retrotranslocation, misfolded luminal proteins first need to traverse the ER membrane before ubiquitination can occur in the cytosol. It was suggested that the membrane-embedded ubiquitin ligase Hrd1 forms a retrotranslocation pore regulated by cycles of auto- and deubiquitination[5–8]. However, the mechanism by which auto-ubiquitination affects Hrd1 and allows polypeptides to cross the membrane and whether Hrd1 forms a membrane-spanning pore remained unknown. Here, using purified Hrd1 incorporated into different model membranes, we show that Hrd1 auto-ubiquitination leads to the opening of a pore. Substrate binding increases the pore size and its activity, whereas deubiquitination closes the pore and renders it unresponsive to substrate. We identify two binding sites for misfolded proteins in Hrd1, a low-affinity luminal site and a high-affinity cytoplasmic site formed following auto-ubiquitination of specific lysine residues in Hrd1's RING domain. We propose that the affinity difference between the luminal and cytoplasmic binding sites provides the initial driving force for substrate movement through Hrd1.

In *Saccharomyces cerevisiae*, ERAD of luminal proteins (ERAD-L) requires the Hrd1 complex, which is composed of the ubiquitin ligase Hrd1, three other membrane proteins (Hrd3, Usa1 and Der1) and the lumen-soluble Yos9 (refs. [9–16]). Ubiquitination depends on the ubiquitin-conjugating enzyme Ubc7 and its cofactor Cue1 (refs. [17–19]) and recruits the Cdc48 complex, which is composed of the ATPase Cdc48 and its cofactors Npl4, Ufd1 and Ubx2. This complex catalyses the extraction of substrates from the ER membrane in an ATP-dependent manner[6,20–25]. Overexpression of Hrd1 obviates the need for the other components of the Hrd1 complex[5,26]. In further support of a crucial role of Hrd1 in retrotranslocation, reconstitution experiments with purified Hrd1 showed that a membrane-anchored version of a misfolded mutant of carboxypeptidase Y (CPY*)[27] is translocated across the membrane when specific lysine residues of Hrd1 are available for auto-ubiquitination[7]. A cryo-electron microscopy structure of Hrd1 in complex with Hrd3 revealed a hydrophilic cavity on the cytoplasmic side of Hrd1 and it was speculated that it represents a closed state of the retrotranslocon[28]. We hypothesized that retrotranslocation-competent Hrd1 forms a water-filled channel under appropriate conditions and is thus suitable for electrophysiological characterization. Protein translocases such as SecY, the protein-conducting channel involved in the translocation of secretory proteins across the bacterial plasma membrane, or the mitochondrial TIM23 presequence translocase show voltage-dependent ion conductance in electrophysiological characterizations[29–31]. In these experiments, electrophysiological parameters such as gating dynamics, pore size and substrate dependency have been used as read-outs for the activity and conformational dynamics of the protein-conducting pores that occur during translocation. Here we combined single-channel electrophysiology with quantitative biochemical analysis to analyse pore formation and substrate engagement by Hrd1.

Purified Hrd1 was reconstituted in large unilamellar vesicles (LUVs; Extended Data Fig. 1a). Proteolytic protection experiments showed that the protein was mostly unidirectionally oriented with the RING domain facing the outside (Extended Data Fig. 1b). When these Hrd1 liposomes were added to planar lipid bilayers (PLBs), no channel activity was observed (Fig. 1a). Next, we incubated Hrd1 liposomes with the ubiquitin-activating enzyme (E1) Uba1, the ubiquitin-conjugating enzyme (E2) Ubc7, a cytoplasmic fragment of Cue1, ATP and ubiquitin (ubiquitination mix), which resulted in efficient Hrd1 auto-ubiquitination (Fig. 1c). Strikingly, when ubiquitinated Hrd1 liposomes were added to PLBs, we observed fusion events that led to mostly small ion currents and occasional gating events (Fig. 1b,d). The vast majority of gating events exhibited small conductance changes in the range of 10–50 pS (Fig. 1e), but occasionally large conductance states of up to 620 pS were observed (Extended Data Fig. 1c). The channels showed a mild cation selectivity that changed depending on the open state of the pore (Extended Data Fig. 1d). No channel activity was observed in experiments lacking ATP or when a different protein bearing polyubiquitin chains was reconstituted (Fig. 1d). To test whether pore formation following auto-ubiquitination was reversible, we next investigated the effect of deubiquitination on channel activity. We inserted auto-ubiquitinated Hrd1 into PLBs and subsequently added the deubiquitinase Usp2 (ref. [32]). Under conditions that led to efficient deubiquitination (Extended Data Fig. 1e), conductance was reduced to the background level recorded in the absence of Hrd1 (Fig. 1f). This behaviour was seen only when Usp2 was added to the *cis* chamber (cytoplasmic side), showing that the orientation of Hrd1 was preserved during osmotically driven fusion, with the cytoplasmic RING domain facing the bilayer *cis* side (Fig. 1g). This shows that non-ubiquitinated Hrd1 is closed. Together, these results establish a regulation mechanism, in which Hrd1 channel formation is controlled by auto- and deubiquitination.

[1]Max Planck Institute for Biophysical Chemistry, Göttingen, Germany. [2]Department of Cellular Biochemistry, University Medical Centre Göttingen, Göttingen, Germany. [3]Department of Structural Dynamics, Max Planck Institute for Biophysical Chemistry, Göttingen, Germany. [4]These authors contributed equally: Vedran Vasic, Niels Denkert. ✉e-mail: alexander.stein@mpibpc.mpg.de; michael.meinecke@med.uni-goettingen.de

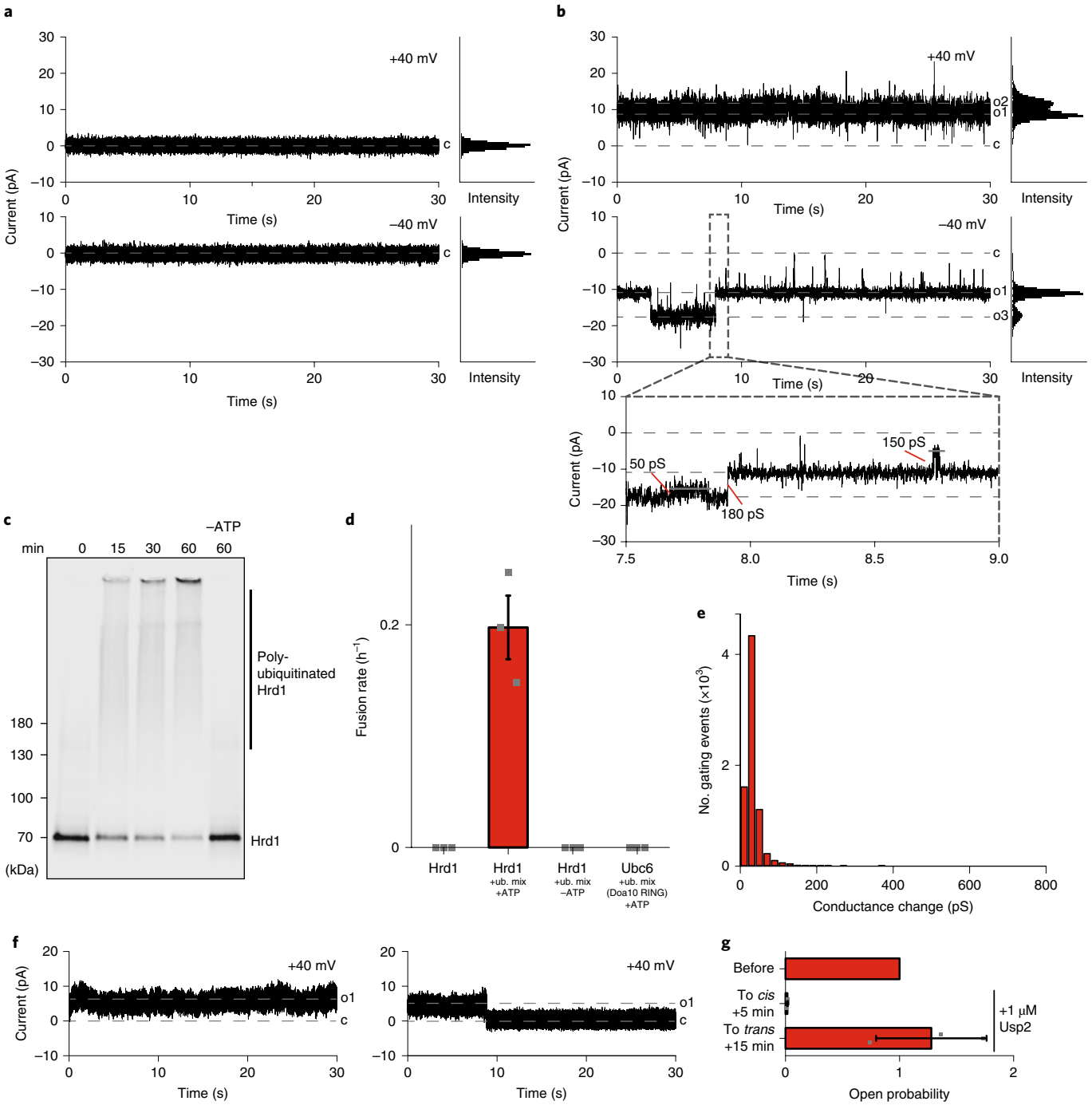

Fig. 1 | Electrophysiological characterization of Hrd1 gating dynamics following auto-ubiquitination. a, The current recordings for PLBs after the addition of liposomes containing non-ubiquitinated Hrd1 at the indicated constant holding potentials (left) and the corresponding point histograms (right). **b**, Current recordings as in **a**, but with polyubiquitinated Hrd1 liposomes. The numbers in the zoomed-in plot indicate various conductance states. **c**, Liposomes containing fluorescently labelled Hrd1 were incubated with ubiquitination mix with or without ATP. Samples from the indicated time points were analysed by SDS–polyacrylamide gel electrophoresis (PAGE) and fluorescence scanning. **d**, Fusion rates of the PLBs with Hrd1 or Ubc6-containing liposomes treated with the indicated conditions. For the quantifications, proteoliposomes were repeatedly added to bilayers and channel fusion events were detected over multiple hours. **e**, A conductance-state histogram of ubiquitinated Hrd1 as calculated from gating transitions that were recorded at varying membrane potentials. **f**, Current recordings of ubiquitinated Hrd1 before (left) and after (right) the addition of 1 μM Usp2 to the *cis* side at the indicated voltages. The closed and various open states of the channels are indicated by c, closed state and o*x*, open states. **g**, The probability of ubiquitinated Hrd1 channels being open before and after side-specific deubiquitination. In **a**–**c**,**f**, representative samples of three independent experiments are shown. In **d**,**g**, the mean ± s.e.m. ($n = 3$ independent experiments) are shown. Source data and unprocessed gels are provided.

We then asked how the presence of a substrate of Hrd1 would influence channel characteristics. The addition of the ERAD model substrate CPY* to bilayer-inserted ubiquitinated Hrd1 resulted in an increased gating frequency and larger conductance changes (Fig. 2a–d). The gating pattern was dynamic with a broad distribution of conductance states (Fig. 2d), with gating events corresponding

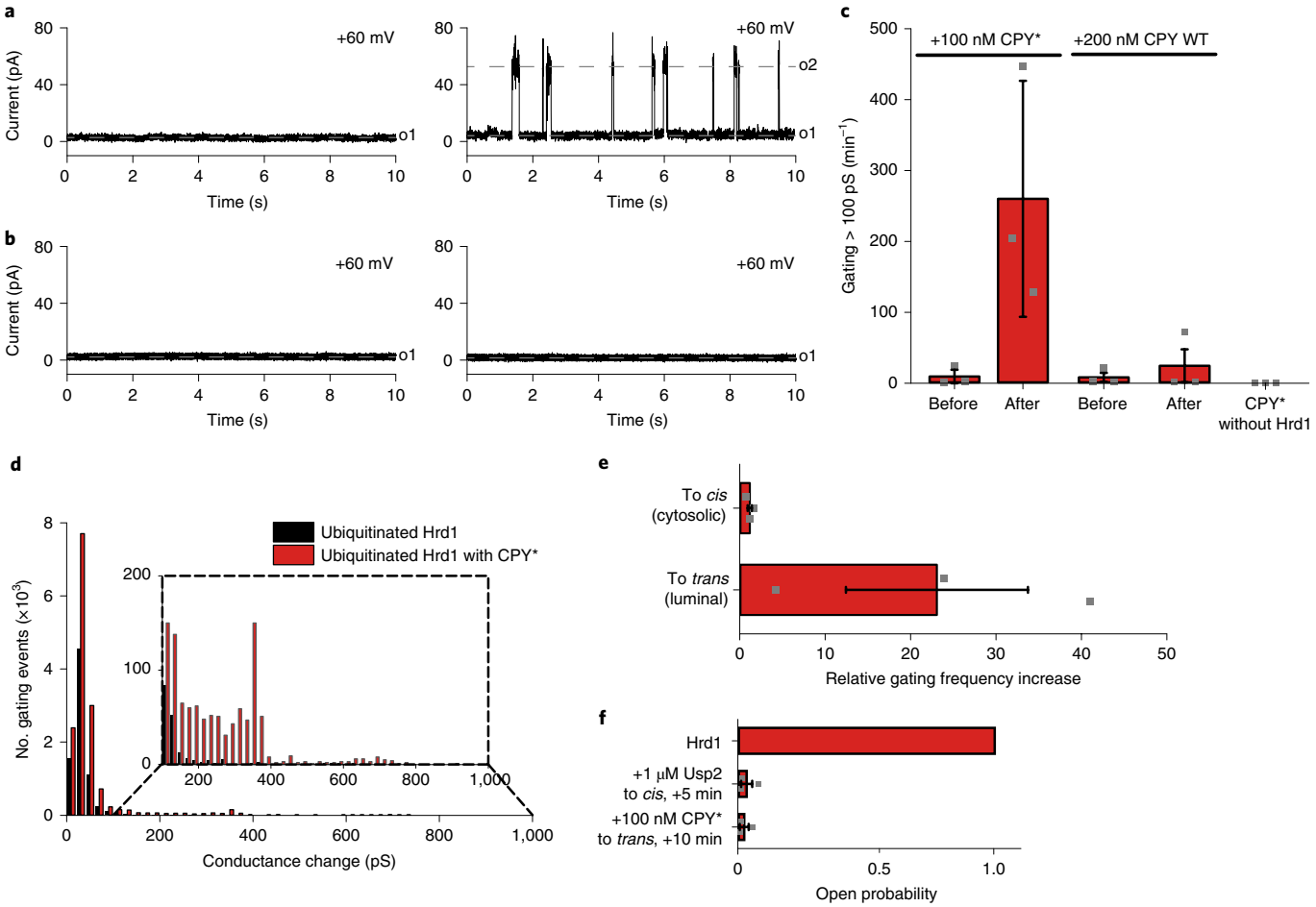

Fig. 2 | Interaction of substrate with ubiquitinated Hrd1 stimulates channel activity. a, Current recordings of ubiquitinated Hrd1 before (left) and after (right) in situ incubation with 100 nM CPY* at the indicated constant holding potential. **b**, Current recordings as in **a**, but using 200 nM CPY WT. In **a**,**b**, representative samples of three independent experiments are shown. **c**, Quantification of the gating activity of ubiquitinated Hrd1 with or without substrate. **d**, Conductance-state histogram of Hrd1 channels after in situ incubation with CPY*, calculated from gating transitions at varying holding potentials (from three independent experiments). The zoomed-in plot illustrates the occurrence of rarer but large gating events, specifically after CPY* addition. **e**, Quantification of the gating activity of Hrd1 channels after side-specific substrate addition of 100 nM CPY*. **f**, The probability of ubiquitinated Hrd1 channels being open before (top) and after (middle) the addition of Usp2 to the indicated chambers, and after the addition of Usp2 followed by the addition of CPY* to the closed channel (bottom). In **c**,**e**,**f**, the mean ± s.e.m. ($n = 3$ independent experiments) are shown. Source data are provided.

to channel diameters of up to 3.5 nm (see Methods), comparable with the dimension of other protein-conducting pores[33,34]. No conductance changes were observed when CPY* was added in the absence of Hrd1 or when wild-type CPY (CPY WT) was added in even higher concentrations to bilayers containing auto-ubiquitinated Hrd1 (Fig. 2b,c). Importantly, CPY* activated Hrd1 channels only when added to the luminal side of the channel (Fig. 2e). When CPY* was added to the luminal side after Hrd1 deubiquitination, the channel remained closed (Fig. 2f). These observations suggest that the interaction of CPY* with auto-ubiquitinated Hrd1 triggers the activation of a Hrd1 retrotranslocation pore that discriminates between misfolded and native proteins at the luminal side, in agreement with our previous observation[6]. Non-ubiquitinated, and hence closed, Hrd1 is unresponsive to substrate.

We next sought to directly investigate the interaction of CPY* with Hrd1 when reconstituted in a lipid bilayer. To this end, we employed proteoliposomes in which only the cytoplasmic side of Hrd1 is accessible. When Hrd1-containing liposomes were immobilized via a streptavidin-binding peptide (SBP) tag to streptavidin magnetic beads and incubated with CPY*, no interaction was observed above background binding to empty beads (Fig. 3a,b). When immobilized Hrd1 liposomes were incubated with ubiquitination mix and then incubated with CPY*, the substrate was efficiently depleted from the supernatant and eluted when biotin was added to dissociate liposomes from beads (Fig. 3a–c for a titration of Hrd1). Incubation with the deubiquitinase Usp2 before substrate incubation abolished binding (Fig. 3a,b). The extent of binding and the apparent affinity of CPY WT were drastically reduced compared to CPY* (Fig. 3c). Similar observations were made when the misfolded variant of yeast proteinase A (PrA*) was used as a substrate (Extended Data Fig. 2a)[27,35]. These results indicate that ubiquitinated Hrd1 specifically binds misfolded proteins on its cytoplasmic side.

As CPY*-dependent channel activation was specific to the luminal side of Hrd1, we next investigated this interaction biochemically with Hrd1 reconstituted in nanodiscs (Extended Data Fig. 2b,c), in which both the cytoplasmic and the luminal side are accessible (Fig. 3d). As non-ubiquitinated Hrd1 in liposomes does not bind CPY*, nanodiscs allowed for differential binding studies. Hrd1 in nanodiscs auto-ubiquitinated with kinetics similar to that observed in liposomes (Fig. 3d,h). Non-ubiquitinated Hrd1 nanodiscs immobilized on beads bound CPY* with an apparent K_D of ~200 nM (Fig. 3e). Following Hrd1 auto-ubiquitination,

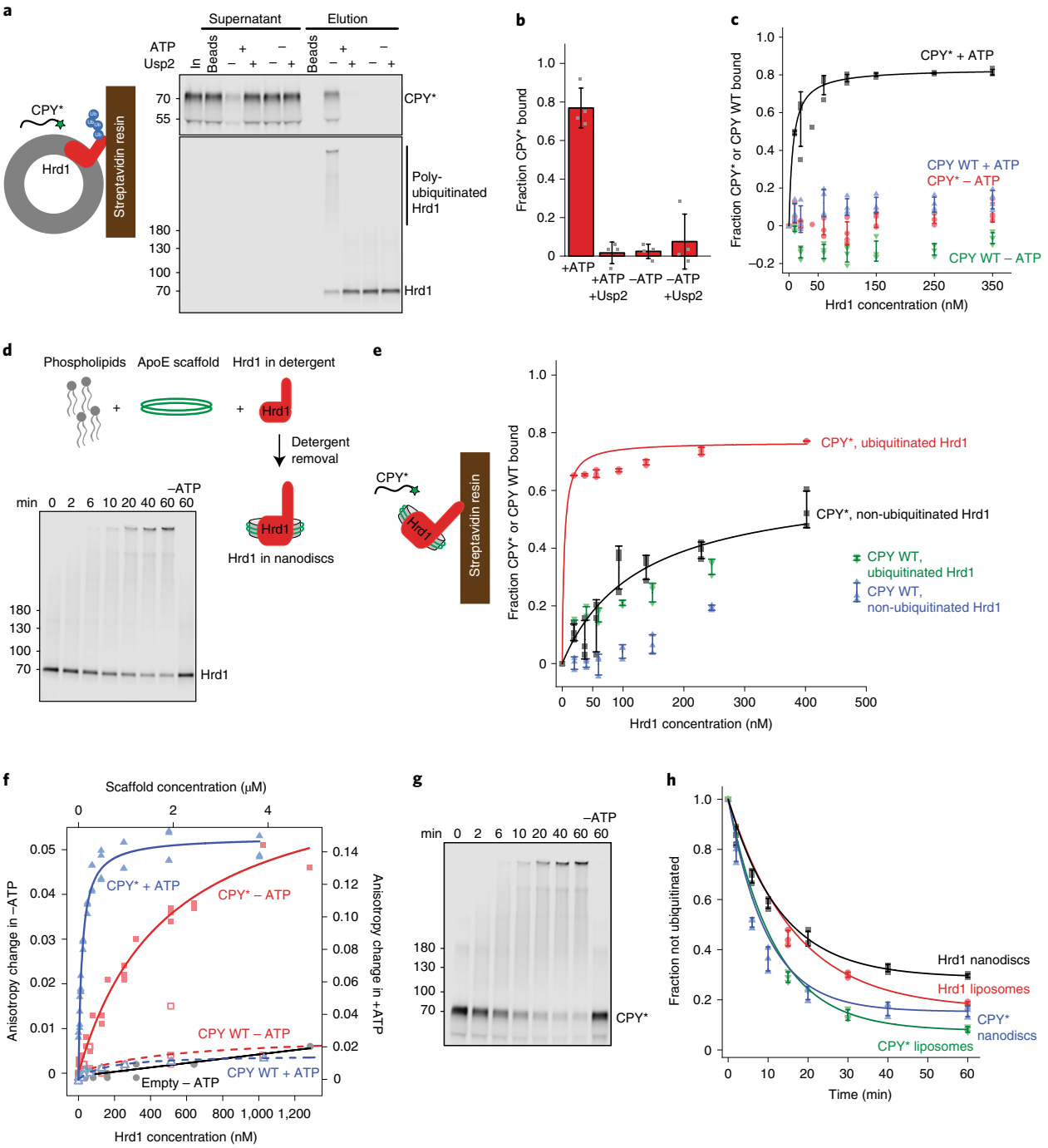

Fig. 3 | Binding of CPY* to the luminal and cytosolic sides of Hrd1. a, Bead-immobilized fluorescently labelled Hrd1 (250 nM) in liposomes was incubated with ubiquitination mix with or without ATP, followed by incubation with fluorescently labelled CPY* (50 nM). Where indicated, Usp2 incubation was performed before incubation with CPY*. The samples were analysed by SDS–PAGE and fluorescence scanning. **b**, The quantification of four experiments from **a**. The mean ± s.d (*n* = 4 independent experiments) are shown. **c**, Experiments performed as in **a**, but with 20 nM of either CPY* or CPY WT and increasing Hrd1 concentrations. The bound fraction was quantified from supernatants and normalized to bead-only controls. The mean ± s.d. (*n* = 4 independent experiments) are shown. **d**, Fluorescently labelled Hrd1 (200 nM) in nanodiscs was incubated with ubiquitination mix with or without ATP. Samples from the indicated time points were analysed by SDS–PAGE and fluorescence scanning. **e**, Fluorescently labelled CPY* or CPY WT (20 nM) was incubated with bead-immobilized fluorescently labelled Hrd1 in nanodiscs that had been treated with ubiquitination mix with or without ATP. The quantification was performed as in **b**. The mean ± s.d. (*n* = 3 independent experiments) are shown. **f**, Fluorescently labelled CPY* or CPY WT (50 nM) was incubated with either empty nanodiscs or Hrd1 nanodiscs (at the concentrations indicated) that had been treated with ubiquitination mix with or without ATP; fluorescence anisotropy was measured. The left and right axes indicate anisotropy changes in the absence and presence of ATP, respectively. The top axis indicates approximate scaffold concentrations. CPY* + ATP: *n* = 4 independent experiments; CPY* – ATP: *n* = 5 independent experiments; CPY WT: *n* = 3 independent experiments; empty nanodiscs: *n* = 2 independent experiments. **g**, Fluorescently labelled CPY* (100 nM) was incubated with fluorescently labelled Hrd1 (200 nM) in nanodiscs and ubiquitination mix with or without ATP. Samples from indicated time points were analysed as before. **h**, The quantification of the ubiquitination experiments performed in **d**,**g**. The mean ± s.d. (*n* = 3 independent experiments) are shown. Source data and unprocessed gels are provided.

CPY* binding with an affinity that was an order of magnitude higher was observed, comparable to results obtained with Hrd1 in proteoliposomes (Fig. 3e). CPY WT showed substantially reduced binding to ubiquitinated and non-ubiquitinated Hrd1 (Fig. 3e). Similar results were obtained when the interaction was measured in solution by fluorescence anisotropy using C-terminally labelled CPY* (Fig. 3f). No interaction with nanodiscs lacking Hrd1 was observed. When either Hrd1 nanodiscs or proteoliposomes were incubated with CPY* in the presence of ubiquitination mix, efficient ubiquitination of CPY* was observed, whereas CPY WT remained largely unmodified (Fig. 3g,h and Extended Data Fig. 2d). Again, similar results were obtained for PrA* with Hrd1 proteoliposomes (Extended Data Fig. 2e). Together, these experiments show that misfolded proteins interact with non-ubiquitinated Hrd1. This interaction probably occurs on the luminal side of Hrd1 because no interaction with non-ubiquitinated Hrd1 was observed in liposomes, where only the cytosolic side is accessible. Auto-ubiquitination of Hrd1 leads to the creation of a high-affinity substrate binding site on its cytoplasmic side. This interaction positions the substrate for efficient ubiquitination.

We sought to further characterize the binding of CPY* to the cytosolic side of ubiquitinated Hrd1 and to distinguish whether interaction occurs through polyubiquitin chains or to Hrd1 directly. To this end, we compared the binding of CPY* to ubiquitinated Hrd1 and to a fusion protein of ubiquitin and Ubc6 (Ub–Ubc6$_{C87A}$, referred to as Ubc6) that is efficiently polyubiquitinated by the RING domain of Doa10 in the presence of Ubc7/Cue1. To also assess the influence of polyubiquitin chain length, ubiquitination reactions were performed in the presence of a K48R ubiquitin mutant, which resulted in the formation of shorter chains attached to either Hrd1 or Ubc6 (Fig. 4a). Titration experiments showed that long polyubiquitin chains were sufficient to mediate an interaction with CPY*, irrespective of whether they were attached to Hrd1 or Ubc6. However, with shorter ubiquitin chains, the apparent affinity for CPY* was significantly greater when chains were attached to Hrd1, indicating that both sites in Hrd1 and on ubiquitin chains contribute to binding (Fig. 4b). The notion that the binding of CPY* to ubiquitinated Hrd1 involves sites in Hrd1 is further corroborated by the observation that deubiquitination releases a substantial fraction of CPY* bound to ubiquitin chains attached to Ubc6, but only a minor fraction is released from deubiquitinated Hrd1 (Extended Data Fig. 3a,b).

Lysine to arginine mutations prevent ubiquitination at the mutation site; in the RING domain of Hrd1 (KRK; see Fig. 4c for an illustration of the nomenclature), they specifically reduce the ERAD of luminal substrates, whereas the degradation of misfolded membrane proteins remains unaffected and ubiquitin ligase activity is maintained[4,7]. To obtain a molecular explanation of this phenotype, we investigated the effect of auto-ubiquitination in specific regions of Hrd1 on both pore formation and substrate ubiquitination. When we reconstituted a Hrd1 mutant lacking lysines in both the RING domain and the C-terminal tail (KRR) in liposomes, auto-ubiquitination was almost completely abolished and CPY* ubiquitination was greatly reduced (Fig. 4d,e). Reintroducing lysines in the RING domain (KKR) recovered about 50% of the auto-ubiquitination activity and almost completely restored CPY* ubiquitination to the levels observed for WT Hrd1 (Fig. 4d,e). By contrast, reintroducing lysines in the C-terminal tail (KRK) failed to restore CPY* ubiquitination (Fig. 4d,e). CPY* binding to Hrd1 correlated with the efficiency of auto- and CPY* ubiquitination (Fig. 4f). A previously described Hrd1 mutant[7] named 3K, in which only three lysine residues in the RING domain were exchanged to arginine (K373, K387 and K407), behaved indistinguishably from the KRK mutant, suggesting that most auto-ubiquitination in the RING domain occurs on these residues (Fig. 4d–f). No binding of CPY WT to Hrd1 mutants was observed and its polyubiquitination was drastically reduced compared to CPY* (Extended Data Fig. 3c–e). Together, these experiments establish that auto-ubiquitination of lysines in the RING domain of Hrd1 is both necessary and sufficient for efficient binding and ubiquitination of the substrate by Hrd1. We observed drastically reduced CPY* binding when multiple mono-ubiquitinations were generated on Hrd1 using the K48R ubiquitin mutant, which indicates that polyubiquitination is required (Extended Data Fig. 3f–h).

Finally, we tested the effect of lysine mutations on Hrd1 channel activity. No channel insertions were observed when auto-ubiquitination was entirely abolished (KRR) or when polyubiquitination was prevented by using the K48R ubiquitin mutant (Fig. 4g). By contrast, when auto-ubiquitination in the RING domain was prevented using the KRK mutant we observed channel activity, but the ion conductance lifetimes were drastically reduced (Fig. 4h,i), indicating decreased stability of the open state of mutant Hrd1 channels. Importantly, no channel reopening in the presence of CPY* was observed for the KRK mutant (Extended Data Fig. 3i). Together, these observations show that auto-ubiquitination in the RING domain of Hrd1 is required for the formation of a stable retrotranslocation pore that is responsive to substrate.

Here we investigated the mechanism of retrotranslocation in ERAD-L. We employed high-resolution electrophysiology to investigate how Hrd1 auto-ubiquitination and interaction with a misfolded substrate affect the formation of a pore on a single-molecule level. Our data show that auto-ubiquitination in the RING domain of Hrd1 has two effects. First, it leads to the opening of a pore and probably primes Hrd1 for the insertion of the substrate from the

Fig. 4 | Auto-ubiquitination in the RING domain of Hrd1 is essential for channel stability, efficient substrate binding and ubiquitination. a, Liposomes containing either fluorescently labelled Hrd1 or an amino-terminal fusion of ubiquitin to Ubc6 (Ub–Ubc6$_{C87A}$, referred to as Ubc6) together with Cue1 were incubated with ubiquitination mix with or without ATP. Increasing concentrations of K48R ubiquitin were added to the ubiquitination mix to generate long, medium (Med.) or short ubiquitin chains. For Ubc6, the RING domain of Doa10 was included in the ubiquitination mix. Samples were analysed by SDS–PAGE and fluorescence scanning. A representative image of three independent experiments with similar results is shown. **b**, Bead-immobilized liposomes were ubiquitinated as in **a** and then incubated with fluorescently labelled CPY* (20 nM). The bound fraction was quantified from the supernatants and normalized to bead-only controls. The concentrations of Hrd1 or Ubc6 plotted on the *x* axis were normalized to the degree of ubiquitination, as determined from bead-eluted samples before incubation with CPY*. $n = 3$ independent experiments. **c**, The nomenclature of the Hrd1 mutants used. **d**, Fluorescently labelled WT Hrd1 or the indicated mutants in liposomes (200 nM) and CPY* (100 nM) were incubated with ubiquitination mix with or without ATP. Samples from the time points indicated were analysed by SDS–PAGE and fluorescence scanning. **e**, A quantification of the experiments performed in **d**. The mean ± s.d are shown ($n = 3$ independent experiments). **f**, Increasing concentrations of ubiquitinated, bead-immobilized WT Hrd1 or the indicated Hrd1 mutants in liposomes were incubated with fluorescently labelled CPY* (20 nM). The bound fraction was quantified from supernatants and normalized to bead-only controls. The mean ± s.d are shown ($n = 3$ independent experiments). **g**, The fusion rates of Hrd1 variants. Hrd1 proteoliposomes were added to bilayers and fusion events were detected for several hours. The mean ± s.e.m. are shown ($n = 3$ independent experiments). **h**, A current recording of the ubiquitinated Hrd1 KRK mutant at the indicated constant holding potential. **i**, A quantification of Hrd1 open-state stability calculated from a lifetime analysis of Hrd1 WT and KRK. $n = 6$ independent experiments for WT and $n = 11$ independent experiments for KRK as shown in **h**. Source data and unprocessed gels are provided.

luminal side, as indicated by changed pore characteristics in the presence of substrate. Second, auto-ubiquitination creates a high-affinity binding site for substrate on the cytoplasmic side of Hrd1. Ubiquitin chains and Hrd1 both contribute to this binding. We propose that this interaction provides the initial driving force for retrotranslocation. Furthermore, binding on the cytoplasmic side

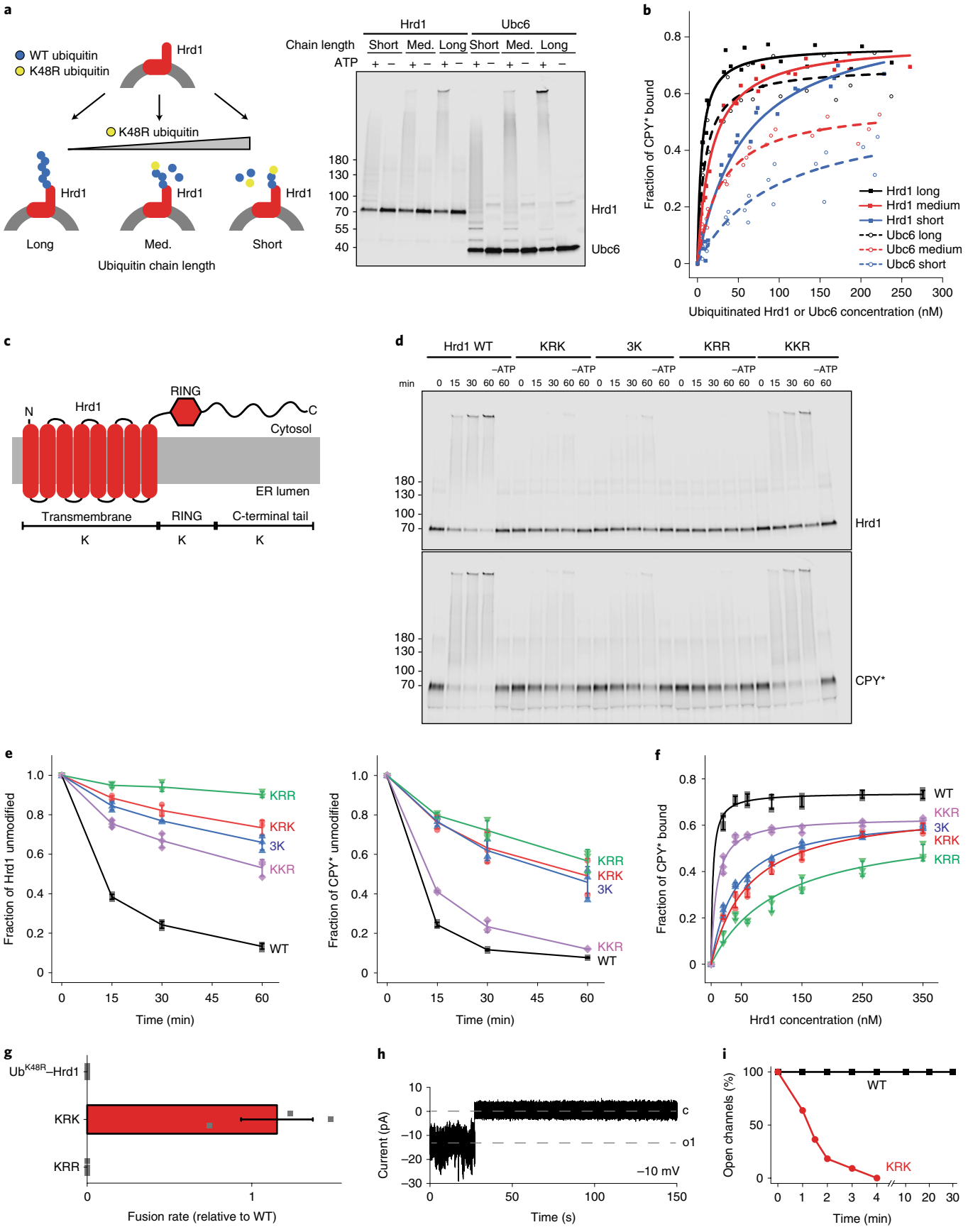

of Hrd1 positions the substrate for efficient ubiquitination, which would recruit the Cdc48 ATPase. Cdc48 action dissociates the tight interaction of CPY* and Hrd1 and ultimately results in the release of the substrate from the membrane[6]. Deubiquitination closes the channel and leaves it insensitive to substrate activation (Extended Data Fig. 4).

Analysing channel formation, substrate binding and ubiquitination with Hrd1 alone allowed us to investigate specific properties of Hrd1. This was motivated by the following findings: overexpression of Hrd1 partially compensates for the absence of Hrd3, Usa1 and Der1[5,26,36]; and Hrd1 auto-ubiquitination is important both in intact cells and in a reconstituted system where Hrd1 is sufficient to bring about retrotranslocation[7,37]. Future reconstitution approaches need to address how Hrd3, Usa1 and Der1 affect retrotranslocation and regulate auto-ubiquitination. In vivo photo-crosslinking experiments showed that the presence of Der1 is required for the interaction of substrate with Hrd1 and that Der1 directly interacts with a retrotranslocating substrate[5,16]. Apart from its role in recruiting Der1 to the HRD complex, Usa1 has been shown to influence the oligomeric state of Hrd1. Mutations that affect the oligomeric state of Hrd1 partially inhibit ERAD[5,38]. A direct contribution of Hrd3 to the retrotranslocation process is more difficult to discern from in vivo experiments because the ablation of Hrd3 renders Hrd1 unstable[39,40]. Overexpression of the deubiquitinase Ubp1 stabilizes Hrd1 and rescues some of the phenotypes of a *hrd3* deletion, supporting a model in which Hrd3 mainly limits Hrd1 auto-ubiquitination[8]. However, other experiments suggested that Hrd3 is intimately linked to retrotranslocation and that its function is not restricted to stabilizing only Hrd1[36]. An attractive model involves Hrd3 acting as a gate-keeper that prevents auto-ubiquitination in the absence of substrate, thus minimizing potentially harmful channel opening and recruitment of the Cdc48 complex to Hrd1.

High-resolution structures of retrotranslocation intermediates are required to understand the structural consequences of auto-ubiquitination. We speculate that auto-ubiquitination affects the structure of the Hrd1 complex either through steric effects or by acting as an allosteric modifier that shifts a conformational equilibrium in Hrd1 to an open, substrate-sensitive state.

Online content

Any methods, additional references, Nature Research reporting summaries, source data, extended data, supplementary information, acknowledgements, peer review information; details of author contributions and competing interests; and statements of data and code availability are available at https://doi.org/10.1038/s41556-020-0473-4.

Received: 29 April 2019; Accepted: 20 January 2020;
Published online: 24 February 2020

References

1. Christianson, J. C. & Ye, Y. Cleaning up in the endoplasmic reticulum: ubiquitin in charge. *Nat. Struct. Mol. Biol.* **21**, 325–335 (2014).
2. Ruggiano, A., Foresti, O. & Carvalho, P. Quality control: ER-associated degradation: protein quality control and beyond. *J. Cell Biol.* **204**, 869–879 (2014).
3. Mehrtash, A. B. & Hochstrasser, M. Ubiquitin-dependent protein degradation at the endoplasmic reticulum and nuclear envelope. *Semin. Cell Dev. Biol.* **93**, 111–124 (2019).
4. Wu, X. & Rapoport, T. A. Mechanistic insights into ER-associated protein degradation. *Curr. Opin. Cell Biol.* **53**, 22–28 (2018).
5. Carvalho, P., Stanley, A. M. & Rapoport, T. A. Retrotranslocation of a misfolded luminal ER protein by the ubiquitin-ligase Hrd1p. *Cell* **143**, 579–591 (2010).
6. Stein, A., Ruggiano, A., Carvalho, P. & Rapoport, T. A. Key steps in ERAD of luminal ER proteins reconstituted with purified components. *Cell* **158**, 1375–1388 (2014).
7. Baldridge, R. D. & Rapoport, T. A. Autoubiquitination of the Hrd1 ligase triggers protein retrotranslocation in ERAD. *Cell* **166**, 394–407 (2016).
8. Peterson, B. G., Glaser, M. L., Rapoport, T. A. & Baldridge, R. D. Cycles of autoubiquitination and deubiquitination regulate the ERAD ubiquitin ligase Hrd1. *eLife* **8**, e50903 (2019).
9. Hampton, R. Y., Gardner, R. G. & Rine, J. Role of 26S proteasome and HRD genes in the degradation of 3-hydroxy-3-methylglutaryl-CoA reductase, an integral endoplasmic reticulum membrane protein. *Mol. Biol. Cell* **7**, 2029–2044 (1996).
10. Knop, M., Finger, A., Braun, T., Hellmuth, K. & Wolf, D. H. Der1, a novel protein specifically required for endoplasmic reticulum degradation in yeast. *EMBO J.* **15**, 753–763 (1996).
11. Bordallo, J., Plemper, R. K., Finger, A. & Wolf, D. H. Der3p/Hrd1p is required for endoplasmic reticulum-associated degradation of misfolded lumenal and integral membrane proteins. *Mol. Biol. Cell* **9**, 209–222 (1998).
12. Bays, N. W., Gardner, R. G., Seelig, L. P., Joazeiro, C. A. & Hampton, R. Y. Hrd1p/Der3p is a membrane-anchored ubiquitin ligase required for ER-associated degradation. *Nat. Cell Biol.* **3**, 24–29 (2001).
13. Gauss, R., Jarosch, E., Sommer, T. & Hirsch, C. A complex of Yos9p and the HRD ligase integrates endoplasmic reticulum quality control into the degradation machinery. *Nat. Cell Biol.* **8**, 849–854 (2006).
14. Carvalho, P., Goder, V. & Rapoport, T. A. Distinct ubiquitin-ligase complexes define convergent pathways for the degradation of ER proteins. *Cell* **126**, 361–373 (2006).
15. Kanehara, K., Xie, W. & Ng, D. T. Modularity of the Hrd1 ERAD complex underlies its diverse client range. *J. Cell Biol.* **188**, 707–716 (2010).
16. Mehnert, M., Sommer, T. & Jarosch, E. Der1 promotes movement of misfolded proteins through the endoplasmic reticulum membrane. *Nat. Cell Biol.* **16**, 77–86 (2014).
17. Hiller, M. M., Finger, A., Schweiger, M. & Wolf, D. H. ER degradation of a misfolded luminal protein by the cytosolic ubiquitin-proteasome pathway. *Science* **273**, 1725–1728 (1996).
18. Biederer, T., Volkwein, C. & Sommer, T. Role of Cue1p in ubiquitination and degradation at the ER surface. *Science* **278**, 1806–1809 (1997).
19. Wilhovsky, S., Gardner, R. & Hampton, R. *HRD* gene dependence of endoplasmic reticulum-associated degradation. *Mol. Biol. Cell* **11**, 1697–1708 (2000).
20. Twomey, E. C. et al. Substrate processing by the Cdc48 ATPase complex is initiated by ubiquitin unfolding. *Science* **365**, eaax1033 (2019).
21. Bays, N. W., Wilhovsky, S. K., Goradia, A., Hodgkiss-Harlow, K. & Hampton, R. Y. HRD4/NPL4 is required for the proteasomal processing of ubiquitinated ER proteins. *Mol. Biol. Cell* **12**, 4114–4128 (2001).
22. Neuber, O., Jarosch, E., Volkwein, C., Walter, J. & Sommer, T. Ubx2 links the Cdc48 complex to ER-associated protein degradation. *Nat. Cell Biol.* **7**, 993–998 (2005).
23. Jarosch, E. et al. Protein dislocation from the ER requires polyubiquitination and the AAA-ATPase Cdc48. *Nat. Cell Biol.* **4**, 134–139 (2002).
24. Ye, Y., Meyer, H. H. & Rapoport, T. A. The AAA ATPase Cdc48/p97 and its partners transport proteins from the ER into the cytosol. *Nature* **414**, 652–656 (2001).
25. Schuberth, C. & Buchberger, A. Membrane-bound Ubx2 recruits Cdc48 to ubiquitin ligases and their substrates to ensure efficient ER-associated protein degradation. *Nat. Cell Biol.* **7**, 999–1006 (2005).
26. Plemper, R. K. et al. Genetic interactions of Hrd3p and Der3p/Hrd1p with Sec61p suggest a retro-translocation complex mediating protein transport for ER degradation. *J. Cell Sci.* **112**, 4123–4134 (1999).
27. Finger, A., Knop, M. & Wolf, D. H. Analysis of two mutated vacuolar proteins reveals a degradation pathway in the endoplasmic reticulum or a related compartment of yeast. *Eur. J. Biochem.* **218**, 565–574 (1993).
28. Schoebel, S. et al. Cryo-EM structure of the protein-conducting ERAD channel Hrd1 in complex with Hrd3. *Nature* **548**, 352–355 (2017).
29. Meinecke, M. et al. Tim50 maintains the permeability barrier of the mitochondrial inner membrane. *Science* **312**, 1523–1526 (2006).
30. Saparov, S. M. et al. Determining the conductance of the SecY protein translocation channel for small molecules. *Mol. Cell* **26**, 501–509 (2007).
31. Truscott, K. N. et al. A presequence- and voltage-sensitive channel of the mitochondrial preprotein translocase formed by Tim23. *Nat. Struct. Biol.* **8**, 1074–1082 (2001).
32. Hospenthal, M. K., Mevissen, T. E. T. & Komander, D. Deubiquitinase-based analysis of ubiquitin chain architecture using Ubiquitin Chain Restriction (UbiCRest). *Nat. Protoc.* **10**, 349–361 (2015).
33. Meinecke, M. et al. The peroxisomal importomer constitutes a large and highly dynamic pore. *Nat. Cell Biol.* **12**, 273–277 (2010).
34. Wirth, A. et al. The Sec61p complex is a dynamic precursor activated channel. *Mol. Cell* **12**, 261–268 (2003).
35. Spear, E. D. & Ng, D. T. Single, context-specific glycans can target misfolded glycoproteins for ER-associated degradation. *J. Cell Biol.* **169**, 73–82 (2005).
36. Vashistha, N., Neal, S. E., Singh, A., Carroll, S. M. & Hampton, R. Y. Direct and essential function for Hrd3 in ER-associated degradation. *Proc. Natl Acad. Sci. USA* **113**, 5934–5939 (2016).

37. Neal, S. et al. The Dfm1 derlin is required for ERAD retrotranslocation of integral membrane proteins. *Mol. Cell* **69**, 306–320 (2018).
38. Horn, S. C. et al. Usa1 functions as a scaffold of the HRD-ubiquitin ligase. *Mol. Cell* **36**, 782–793 (2009).
39. Gardner, R. G. et al. Endoplasmic reticulum degradation requires lumen to cytosol signaling. Transmembrane control of Hrd1p by Hrd3p. *J. Cell Biol.* **151**, 69–82 (2000).
40. Carroll, S. M. & Hampton, R. Y. Usa1p is required for optimal function and regulation of the Hrd1p endoplasmic reticulum-associated degradation ubiquitin ligase. *J. Biol. Chem.* **285**, 5146–5156 (2010).

Methods

Strains. All Hrd1 variants were expressed in an *S. cerevisiae ubc7* knockout strain derived from BY4742 (OpenBiosystems; MATα Ura3Δ0 His3Δ1 Leu2Δ0 Lys2Δ0 *ubc7*::*KANR*). For the expression of ERAD substrates, an *S. cerevisiae* strain lacking *hrd3* and *alg3*, derived from BY4741 (OpenBiosystems), was used (MATa *ura3Δ0 his3Δ1 leu2Δ0 lys2Δ0 hrd3*::*KANR alg3*::*HIS3*). Uba1 was expressed in strain InvSc1 (Invitrogen). The catalytic domain of the human deubiquitinase Usp2, as well as Ubc6, Ubc7, the cytoplasmic fragment of Cue1 (Cue1-c), full-length Cue1 and Doa10 RING, all from *S. cerevisiae*, were expressed in the *E. coli* strain BL21-CodonPlus (DE3)-RIPL (Agilent).

Plasmids. Hrd1 and its mutants contained a C-terminal SBP tag preceded by a tobacco etch virus (TEV) cleavage site; they were cloned into pRS426-Pgal1 as previously described[6].

CPY*, containing the G255R point mutation[27], was cloned into the pRS425-pGal1 expression vector with a C-terminal His_{14} tag. The CPY signal sequence was replaced by the α-factor signal sequence. Furthermore, a human influenza hemagglutinin (HA) tag for detection, the sortase labelling tag LPETGG and the ER-retention signal HDEL were included at the C terminus. The resulting fusion protein was CPY*–HA–His_{14}–LPETGG–HDEL. The expression construct for CPY WT was as previously described[6], except that the C-terminal SBP tag was removed by site-directed mutagenesis, resulting in the sequence His_{14}–3C–CPY WT–LPETGG.

PrA WT, encoded by *pep4*, was amplified from genomic DNA and cloned into pRS426-pGal1 with C-terminal His_{14} and LPETGG tags. To make PrA* with C-terminal His_{14} and LPETGG tags, the sequence encoding amino acids 54–92 of PrA WT was deleted by site-directed mutagenesis[27,35].

Usp2, with an N-terminal His_6 tag in the pET28a vector, was a gift from C. Arrowsmith (Addgene plasmid no. 36894).

To clone a construct for the expression of Ub–$Ubc6_{C87A}$ (referred to as Ubc6), the sequence encoding $ubiquitin_{V76}$ (amino acids 1–76) was inserted between the sequence encoding the His_{14}–SUMO tag and $Ubc6_{C87A}$. For efficient Ulp1 cleavage, a linker sequence (coding for GSG) was inserted between the His_{14}–SUMO tag and ubiquitin. The construct also contained a C-terminal tag for sortase-mediated labelling (coding for LPETGG).

The construct for the expression of full-length Cue1 was engineered with an N-terminal His_{14}–SUMO tag and a C-terminal TEV cleavage site followed by an SBP tag separated from Cue1 by a linker. A short linker (coding for SGS) was introduced between the His_{14}–SUMO tag and Cue1. The coding sequence for this construct was inserted into the pET39b(+) vector (Novagen) immediately after the DsbA signal sequence. After TEV cleavage during purification, the sequence for the C-terminal end of Cue1 was GSGENLYFQ.

The *S. cerevisiae* sequence encoding the first 129 amino acids of Doa10 was cloned into K27SUMO (ref. [6]) including a C-terminal hexa-histidine tag.

ApoE422K (kindly provided by O. D. Bello and J. E. Rothman) was recloned into K27SUMO.

Protein purification. All purifications were performed at 4 °C or on ice unless otherwise indicated. The E1 enzyme Uba1, Ubc7 and the cytoplasmic fragment of Cue1 (all from *S. cerevisiae*) were purified as described[6].

Hrd1. The expression and purification of Hrd1 and Hrd1 mutants was essentially performed as described[6], with some modifications in the preparation of the membrane fraction. Briefly, 100–150 g of cells was resuspended in 900 ml cold MilliQ water supplemented with 2 mM DTT and incubated for 15 min on ice. Cells were pelleted at 3,000*g* for 10 min at 4 °C and resuspended in buffer M_F (20 mM HEPES–KOH pH 7.5, 5 mM potassium acetate, 600 mM mannitol, 0.5 mM EDTA) supplemented with 1 mM phenylmethanesulfonyl fluoride (PMSF) and 2 μM pepstatin A. Cells were lysed with zirconia glass beads (one third of the volume of the cell suspension) in a bead beater (BioSpec) with cycles of 15-s on, 1-min off for 50 min. The beads were filtered off and the lysate was centrifuged at 1,500*g* for 10 min. The supernatant was recovered and centrifuged at 30,000*g* for 45 min. The supernatant was discarded and the pellet was resuspended in buffer M_F by douncing. This crude membrane fraction was washed twice by repelleting at 40,000 r.p.m. for 30 min in a Ti45 rotor (Beckman). The pellet was finally resuspended by douncing in a minimal amount of buffer M_F and flash frozen in liquid nitrogen. The frozen membrane fraction was stored at −80 °C until further use. For affinity purification, the membrane fraction was washed in buffer H (50 mM HEPES–KOH pH 7.4, 300 mM KCl, 5 mM magnesium acetate, 0.5 mM tris(2-carboxyethyl)phosphine (TCEP)) as described above. The pellet was resuspended in buffer H to approximately 3–4 mg ml^{-1} total protein concentration. Decyl maltose neopentyl glycol (DMNG; Anatrace) was added to 1% (weight/volume; w/v) and the solution was stirred for 1 h at 4 °C. The lysate was cleared by centrifugation at 40,000 r.p.m. for 30 min in a Ti45 rotor and 3 ml high-capacity streptavidin agarose resin (Pierce) was added, followed by incubation for 3 h at 4 °C. Beads were filtered off and washed with 20 column volumes (CVs) of buffer H with 1 mM DMNG, 20 CVs of buffer H with 0.12 mM DMNG, 10 CVs of room temperature buffer H with 0.12 mM DMNG and 0.25 mM ATP, and finally 60 CVs of buffer H with 0.12 mM DMNG. Hrd1 was eluted with buffer H supplemented with 2 mM biotin. The protein was further purified on a Superose 6 XK 16/70 column (GE Healthcare) equilibrated with buffer H containing 0.12 mM DMNG. Peak fractions were pooled and concentrated in a 100-kDa-cut-off centrifugal filter (Amicon, Millipore). Aliquots were flash frozen and stored at −80 °C.

CPY.* Expression of CPY* was performed as described[6]. CPY* was purified from a membrane fraction. To prepare the membrane fraction, the cell pellet was resuspended in approximately 150 ml buffer M_C (50 mM HEPES–KOH pH 7.4, 300 mM KCl), supplemented with 1 mM PMSF and 2 μM pepstatin A. Bead beating was performed as with Hrd1. Glass beads were filtered off and the lysate was centrifuged at 2,000*g* for 10 min. The supernatant was centrifuged at 40,000 r.p.m. in a Ti45 rotor for 45 min and the pellet was washed with 200 ml buffer M_C. The resulting pellet was resuspended in a minimal amount of buffer M_C, flash frozen and stored at −80 °C. For purification of CPY*, the membrane fraction was washed once in buffer M_C and centrifuged again (40,000 r.p.m., Ti45 rotor, 30 min). The pellet was resuspended in 250 ml buffer S_C (50 mM HEPES–KOH pH 7.4, 300 mM KCl, 1 mM magnesium acetate, 1 mM TCEP, 40 mM imidazole, 6 M urea) and stirred for 1 h. Insoluble material was removed by centrifugation at 40,000 r.p.m. for 30 min in a Ti45 rotor. The supernatant was loaded on a HisTrap HP 5-ml column (GE Healthcare) equilibrated with buffer S_C. The column was washed with 30 CVs buffer W_C (25 mM HEPES–KOH pH 7.4, 300 mM KCl, 1 mM magnesium acetate, 0.5 mM TCEP, 40 mM imidazole, 2 mM Fos-choline-13 (Anatrace)). CPY* was eluted with buffer I_C (25 mM HEPES–KOH pH 7.4, 300 mM KCl, 1 mM magnesium acetate, 0.5 mM TCEP, 400 mM imidazole, 2 mM Fos-choline-13). Peak fractions were pooled and concentrated in a 30-kDa-cut-off centrifugal filter. The eluted CPY* was sortase-labelled with DyLight 800 and further purified on a Superdex 200 increase 10/300 GL column equilibrated with buffer L_C (20 mM HEPES–KOH pH 7.4, 300 mM KCl, 1 mM magnesium chloride, 1 mM DTT, 2.5 M urea).

CPY WT. CPY WT was expressed as described[6]. To purify CPY WT, a membrane fraction was prepared as described for CPY*, with the exception that only one round of bead beating was performed. The membrane fraction was washed with approximately 200 ml buffer M_C and centrifuged at 40,000 r.p.m. in a Ti45 rotor for 30 min. The membrane fraction was then solubilized in buffer M_C containing 2% (w/v) *n*-decyl-β-D-maltopyranoside (DM; Glycon Biochemicals) and 30 mM imidazole for 30 min at 4 °C. The unsolubilized material was cleared by centrifugation at 40,000 r.p.m. in a Ti45 rotor for 30 min. The supernatant was loaded onto a 5-ml HisTrap FF column (GE Healthcare) and the detergent was removed by washing with 30 CVs buffer M_C without DM (containing 30 mM imidazole). The protein was eluted with buffer M_C supplemented with 400 mM imidazole. β-mercaptoethanol (5 mM) was added to the eluted protein and the His_{14} tag was cleaved with 3C protease (1:20 molar ratio of protease to CPY WT, overnight at 4 °C). CPY WT was sortase labelled with DyLight 800 followed by gel filtration on a Superdex 200 increase 10/300 GL column equilibrated with 20 mM HEPES–KOH pH 7.4, 300 mM NaCl, 5 mM β-mercaptoethanol.

ApoE422K. ApoE422K expression was performed at 25 °C for 3 h after induction with 0.5 mM isopropyl-β-D-thiogalactoside (IPTG). Cells from a 6-l culture were resuspended in buffer containing 50 mM Tris–HCl, pH 8.0, 500 mM NaCl, 30 mM imidazole, and lysed using a microfluidizer. The lysate was cleared by ultracentrifugation, supplemented with 8 ml washed HisPur resin (Thermo Fisher Scientific) and incubated for 2.5 h with rotation. Beads were filtered off and washed with the same buffer. For the elution, beads were resuspended in three times the bead volume, Ulp1 protease was added to 0.5 μM and the mixture incubated for 1 h with rotation. Eluted protein was dialysed against buffer containing 20 mM Tris–HCl pH 8.0, 100 mM NaCl. The protein was further purified by anion exchange chromatography using a MonoQ 10/100 GL column (GE Healthcare). Protein was eluted in a Tris-buffered linear NaCl gradient from 0.1 to 1 M over 15 CVs. Pooled fractions were dialysed against buffer containing 20 mM HEPES–KOH pH 7.5, 150 mM NaCl, and the final protein concentration was adjusted to 400 μM.

Ubc6. Expression in Terrific Broth was induced with 0.5 mM IPTG and cells were grown at 18 °C for 18 h after induction. Cells were harvested at 4,000 r.p.m., resuspended in buffer I30 (50 mM Tris–HCl pH 8.0 (at 4 °C), 500 mM NaCl, 30 mM imidazole) and stored at −20 °C.

To prepare a membrane fraction, the cells were lysed using a microfluidizer (17,000 psi, two passages). Immediately afterwards, 1 mM PMSF was added. Cell debris and unbroken cells were pelleted (1,500*g*, 10 min). A membrane fraction was prepared by ultracentrifugation of the supernatant (40,000 r.p.m., 45 min, 4 °C, Ti45 rotor). The pellet was resuspended in buffer I30 by douncing, snap frozen in liquid nitrogen and stored at −80 °C. The membrane fraction was solubilized with 1% (w/v) *n*-dodecyl β-maltoside (DDM; Glycon Biochemicals) in buffer containing 50 mM Tris–HCl pH 8.0 (at 4 °C), 500 mM NaCl, 30 mM imidazole and 1 mM PMSF. After solubilization for 1 h, insoluble material was pelleted by ultracentrifugation at 40,000 r.p.m. for 30 min (Ti45 rotor). The supernatant was incubated with HisPur Ni-NTA resin (Thermo Fisher Scientific; 6 ml for 6-l culture) for 2–3 h. Beads were filtered off and washed with 4 × 50 ml wash buffer (20 mM Tris–HCl pH 8.0 (at 4 °C), 500 mM NaCl, 30 mM imidazole, 0.03% (w/v)

DDM). Ubc6 was eluted from the beads by cleavage with the SUMO protease Ulp1. To do this, 1 µM Ulp1 was added to beads resuspended in wash buffer and incubated for 30 min. Beads were filtered off and DTT was added to 10 mM. Protein was further purified by size-exclusion chromatography using a Superdex 200 HiLoad 16/60 column (GE Healthcare) equilibrated with 20 mM HEPES–KOH pH 7.4, 250 mM NaCl, 0.03% (w/v) DDM, 0.2 mM TCEP.

Full-length Cue1. To purify full-length Cue1, expression was induced with IPTG as for Ubc6. The membrane fraction was prepared using the protocol described for Ubc6, but under reducing conditions (buffer C: 20 mM HEPES–KOH pH 7.4, 250 mM NaCl, 250 mM sucrose, 2 mM EDTA, 1 mM DTT). The membrane fraction was solubilized with 1.5% (w/v) DM for 30 min in buffer C. After pelleting non-solubilized material (40,000 r.p.m., 30 min in a Ti45 rotor), the supernatant was incubated with Pierce high-capacity streptavidin agarose slurry (4 ml for 6-l culture) in the presence of 50 nM Ulp1 to cleave off the His_{14}–SUMO tag, and incubated for 1 h. Beads were filtered off and washed with 4 × 25 ml buffer C supplemented with 6 mM DM. Cue1 was eluted with buffer C supplemented with 2 mM biotin. The elution fractions were incubated with 1 µM TEV protease overnight. Cue1 was further purified by size-exclusion chromatography using a Superdex 200 HiLoad 16/60 column (GE Healthcare) equilibrated with 20 mM HEPES–KOH pH 7.4, 250 mM NaCl, 5 mM DM, 1 mM TCEP.

Doa10 RING. Expression in Terrific Broth was induced with 0.5 mM IPTG and cells were grown at 18 °C for 18 h after induction. Cells were lysed as before in buffer containing 50 mM Tris–HCl pH 8.0, 500 mM NaCl, 30 mM imidazole, and the lysate was cleared by ultracentrifugation. HisPur resin (Thermo Fisher Scientific) was added and the suspension incubated for 2.5 h with rotation. Beads were filtered off and washed with the same buffer. Protein was eluted from the column with the same buffer, except that it contained 500 mM imidazole. Eluted protein was supplemented with 0.5 mM DTT and 0.5 µM Ulp1 to cleave off the N-terminal His_{14}–SUMO-tag, followed by dialysis against buffer containing 20 mM Tris–HCl, 100 mM NaCl. The protein was further purified by anion exchange chromatography using a MonoQ column (GE Healthcare) and gel filtration using a Superdex 75 column.

Sortase labelling with fluorescent dyes. All proteins containing the C-terminal LPETGG tag were labelled by sortase-mediated transpeptidation[41]. Briefly, a short peptide with the sequence GGGC (Thermo Fisher Scientific) was labelled with DyLight 680 maleimide, DyLight 800 maleimide or Alexa Fluor 488 C_5 maleimide (Thermo Fisher Scientific). To this end, a 1.5-fold molar excess of GGGC peptide dissolved in 100 mM HEPES–KOH pH 7.4 was added to the lyophilized maleimide-conjugated dye. The reaction was incubated for 1 h at room temperature and was quenched by the addition of 10 mM DTT. The labelled peptide was added in a 5–7-fold molar excess with the LPETGG-tagged protein along with 10 mM $CaCl_2$ and 15 µM sortase A pentamutant from *Staphylococcus aureus*[42]. The reaction was incubated at 4 °C for 16 h and the labelled protein was further purified by size-exclusion chromatography (Superose 6 increase 10/300 GL for Hrd1 and Superdex 200 increase 10/300 GL for CPY* and other substrates). The labelling efficiency ranged between 15 and 60%.

Reconstitution of Hrd1 into liposomes. Hrd1 was reconstituted into preformed LUVs containing the following lipids: 1-palmitoyl-2-oleoyl-glycero-3-phosphocholine (POPC), 1,2-dioleoyl-*sn*-glycero-3-phosphoethanolamine (DOPE), 1,2-dioleoyl-*sn*-glycero-3-phospho-L-serine (DOPS) and cholesterol. All lipids were purchased in powder form from Avanti Polar Lipids and were dissolved in chloroform before use.

LUVs were prepared essentially as described before[43]. Briefly, chloroform stocks of POPC, DOPE, DOPS and cholesterol were mixed at a molar ratio of 6:2:1:1, respectively. Chloroform was removed by evaporation in a rotary evaporator at 20 mbar. The resulting lipid film was dissolved in 1 ml diethyl ether followed by the addition of 300 µl buffer L (20 mM HEPES–KOH pH 7.4, 150 mM potassium chloride, 5 mM magnesium acetate). The solution was sonicated with a tip sonicator on ice to create an emulsion. Diethyl ether was removed at 500 mbar for 10 min, followed by the addition of 700 µl buffer L. The remaining diethyl ether was removed at 300 mbar for 1 h. The resulting lipid suspension was extruded 11 times through a 0.4-µm polycarbonate filter and then 21 times through a 0.1-µm polycarbonate filter (Mini extruder kit, Avanti Polar Lipids). The resulting lipid concentration was 20 mM. For experiments in which Hrd1 ubiquitination was compared to Ubc6, 2% 1,2-dioleoyl-*sn*-glycero-3-phosphoethanolamine-*N*-(biotinyl) (biotinyl PE, Avanti Polar Lipids) was included in the lipid mix.

To reconstitute Hrd1, 4 mM preformed LUVs was destabilized by the addition of 6 mM DMNG along with 1 mM TCEP. Hrd1 was added at a protein:lipid ratio of 1:2,000 (2 µM). The solution was incubated for 1 h at room temperature and DMNG was subsequently removed by application to two successive Pierce detergent removal spin columns (Thermo Fisher Scientific), pre-equilibrated with buffer L + 1 mM TCEP. Incubation in the detergent removal spin columns was performed at room temperature for 15 min. Each preparation resulted in 100–150 µl Hrd1 liposomes. For PLB experiments, Hrd1 was reconstituted at a protein:lipid ratio of 1:1,000 with a final lipid concentration of 8 mM, and detergent was removed with three successive detergent removal spin columns.

The insertion of Hrd1 into liposomes was assessed by flotation in a Nycodenz step gradient. Briefly, 50 µl liposomes was mixed with 50 µl 80% (w/v) Nycodenz (Alere Technologies) prepared in buffer L. 40 µl each of 30% Nycodenz, 15% Nycodenz and buffer L were overlaid stepwise. The density gradient was centrifuged at 50,000 r.p.m. in a S55-S swinging bucket rotor (Thermo Fisher Scientific) for 1 h at 4 °C. Six fractions of 36.7 µl were collected from the top of the gradient. Fractions were analysed by SDS–PAGE and fluorescence scanning with an Odyssey CLx scanner (Li-COR). Liposomes were visible as a sharp band localized primarily in the second fraction from the top after centrifugation.

The orientation of Hrd1 in liposomes was assayed by a protease protection assay using TEV protease. The TEV cleavage site is located on the C terminus of Hrd1, before the SBP tag and fluorescent dye. Hrd1 liposomes were diluted 1:5 into buffer L supplemented with 0.5 mM TCEP and incubated with 0.2 mg ml^{-1} TEV protease for 30 min at room temperature. As a positive control, 6 mM DMNG was included to solubilize the liposomes. Reactions were stopped by the addition of SDS sample buffer and analysed by SDS–PAGE and fluorescence scanning in an Odyssey CLx scanner (Li-COR).

Reconstitution of Ubc6 and Cue1 into liposomes. To reconstitute Ubc6 and full-length Cue1 into liposomes, 4 mM preformed LUVs containing 2% biotinyl PE was mixed with 25 mM *n*-octyl β-D-glucopyranoside (Glycon Biochemicals) along with 0.5 mM TCEP in a total volume of 300 µl. 2 µM Ubc6 and 2 µM Cue1 were added to this mixture and incubated for 1 h at room temperature. Detergent was removed by overnight dialysis against 300 ml buffer L + 0.5 mM TCEP in a 2K MWCO Slide-A-Lyzer dialysis cassette (Thermo Fisher Scientific), with 1 g Bio-Beads SM-2 (Bio-Rad) added to the dialysis buffer.

Reconstitution of Hrd1 into nanodiscs. Nanodiscs were prepared using ApoE422K as a scaffold[44]. POPC (Avanti Polar Lipids) was dissolved in chloroform and dried in a rotary evaporator at 20 mbar. The resulting lipid film was solubilized in 20 mM HEPES, 150 mM NaCl, 2% (w/v) DM (Glycon Biochemicals) to a final POPC concentration of 10 mM. For nanodisc preparation, 500 µl POPC–DM micelles were mixed with 31.25 µM ApoE422K and 10 µM Hrd1 in a total volume of 1 ml, and incubated for 16 h at 4 °C. DM was removed by the addition of 200 mg detergent removal resin (Thermo Fisher Scientific), and incubation for 20 min with rotation and removal of the resin using a spin column. This was repeated three times. The resulting solution was loaded onto a 10–30% (w/v) glycerol gradient prepared using a Gradient Master (Biocomp Instruments). The gradient was centrifuged in a Beckmann SW32Ti rotor for 20 h at 4 °C, fractionated using a peristaltic pump in 20 fractions of approximately 1.5 ml and analysed by SDS–PAGE and Coomassie blue staining. Fractions containing Hrd1 were pooled and concentrated to 1–2 µM Hrd1 using a 100-kDa-cut-off centrifugal filter (Amicon, Millipore) followed by dialysis to remove glycerol. The final Hrd1 concentration was determined using a Hrd1 standard by SDS–PAGE, staining with InstantBlue (Expedeon) and scanning the gel using an Odyssey CLx scanner.

Electrophysiological experiments. The channel-forming properties and pore dynamics of Hrd1 were assessed using the PLB electrophysiological technique, described in detail previously[45–47].

Channel insertion by osmotically driven fusion. The ability to measure ion conductance in PLBs relies on two things. First, a channel-containing liposome has to fuse with the bilayer and, second, this channel needs to open for at least some time to be differentiated from a bilayer containing no channels. In the first case, it has been shown many times that proteoliposomes fuse with PLBs mainly through osmotically driven fusion. For fusion, the *cis* chamber has a higher salt concentration than the *trans* chamber, which leads to a flux of water from the *trans* to *cis* sides. After the attachment of liposomes to the bilayer, a water flux into the proteoliposomes causes liposome swelling and eventually fusion[48]. This process occurs only when proteoliposomes have similar ion concentrations to the *cis* side to which they are added. Channel reconstitution is carried out under different buffer conditions from the fusion experiments. So, for an equilibration of the proteoliposome lumen and the *cis* chamber, open channels are a prerequisite.

Ubiquitin-dependent channel formation and basic characterization. Proteoliposomes containing Hrd1 were preincubated with ubiquitination mix with or without ATP, as described in the text. For osmotically driven fusion, asymmetrical buffer conditions, with 250 mM KCl, 10 mM MOPS–Tris, pH 7.0 in the *cis* chamber and 20 mM KCl, 10 mM MOPS–Tris, pH 7.0 in the *trans* chamber, were established. The proteoliposomes were then deposited next to the lipid bilayer, from the *cis* side, to enable the fusion of liposomes with the bilayer. After fusion, symmetrical buffer conditions were established by perfusion with 20 chamber volumes of the 250-mM KCl buffer and currents were recorded at the indicated voltages.

Conductance states. For conductance-state histograms, conductance differences during gating events under various constant voltages (voltage clamps) were plotted against their frequency. To better visualize the large conductance states that occurred with low frequencies, zoomed-in plots were used (Fig. 2d and Extended Data Fig. 1c).

Channel diameter. The diameter of the pore was calculated from measured stable conductance states. Therefore, we took a cylindrical pore with a restriction zone of 1 nm in length as the basis and assumed a fivefold higher solution resistance within the pore than in the bulk medium as described before[49].

Selectivity determination. To measure the reversal potential (as shown in Extended Data Fig. 1d) of a channel, 12.5-fold asymmetrical buffers were re-established by 20-fold perfusion of the buffer in the *trans* chamber. The ion selectivity was calculated using the Goldman–Hodgkin–Katz equation[50]. Arrows in Extended Data Fig. 1d indicate different reversal potentials at different open states of Hrd1 channels. The numbers give the calculated relative selectivity for the permeabilities (P) of potassium (K^+) and chloride (Cl^-) p_{k^+} over p_{cl^-}.

Substrate-specific activation of Hrd1 channels. For in situ substrate and enzyme interactions, proteins were added to the indicated side of the bilayer at the specified concentration under symmetrical buffer conditions. The buffer in both chambers was then mixed for 2 min by magnetic stirrers and left to rest for 2 min before recordings were resumed.

Determination of channel lifetime. For the determination of the channel lifetimes for Hrd1 WT and mutant forms, the time between channel insertion into the bilayer and spontaneous closure as measured as conductance disappearance was registered. $n=6$ for Hrd1 WT and $n=11$ for the Hrd1 KRK mutant.

Determination of fusion rates of various Hrd1 constructs under indicated conditions. For fusion experiments (Figs. 1d and 4g), proteoliposomes were applied to the bilayer for 20 h per replicate, to a total of 60 h, and fusion events were registered.

Electrophysiological set-up. Current recordings were performed with two Ag/AgCl electrodes that were embedded in a 2 M KCl agar bridge in glass tubes, connected to a headstage (CV-5-1GU), with the *cis* electrode acting as the ground. Signals were amplified by a Geneclamp 500B current amplifier, digitized by a Digidata 1440A A/D converter and recorded with AxoScope 10.3 and Clampex 10.3 software (all Molecular Devices). Data were analysed using the R package stepR (version 2.0-4) (ref. [51]) and OriginPro 8.5 (OriginLab).

Ubiquitination assays. The ubiquitination of Hrd1 variants in liposomes or nanodiscs, and substrate, was performed in buffer U (20 mM HEPES–KOH pH 7.4, 150 mM potassium chloride, 5 mM magnesium acetate, 0.5 mM TCEP, 1 mg ml^{-1} bovine serum albumin (BSA; PanReac AppliChem A1391)) at 30 °C. Liposomes were diluted 1:10 with ubiquitination mix to a final volume of 50 µl, containing final concentrations of 0.2 µM Uba1, 2 µM Ubc7, 2 µM Cue1-c and 100 µM ubiquitin. The final Hrd1 concentration was 200 nM and the final substrate concentration was 100 nM. The reaction was pipetted on ice and initiated by adding 2.5 mM ATP. After pipetting the 0-min time point sample into SDS sample buffer, the reaction was shifted to 30 °C and samples from the indicated time points were pipetted into SDS sample buffer. As a control, reactions were incubated for 1 h in ubiquitination mix lacking ATP. Samples were analysed by SDS–PAGE and fluorescence scanning using an Odyssey CLx scanner (Li-COR). Quantification of non-ubiquitinated Hrd1 and substrate was performed using Image Studio software (Li-COR). Quantifications were performed from three independent experiments. Error bars indicate standard deviation. In Fig. 3h, the data were fitted with a one-phase exponential decay function using Origin software.

Binding assays on beads. For binding experiments, increasing concentrations of Hrd1 liposomes or Hrd1 nanodiscs were immobilized onto magnetic streptavidin beads (Pierce) prewashed with 10 CVs of buffer B_a (20 mM HEPES–KOH pH 7.4, 150 mM potassium chloride, 5 mM magnesium acetate, 0.5 mM TCEP, 2 mg ml^{-1} BSA). Importantly, relatively high concentrations of BSA during the initial washes were necessary to minimize non-specific substrate interaction with the beads. Binding of Hrd1 to beads was performed at room temperature for 1 h. The beads were then washed with buffer B with 0.2 mg ml^{-1} BSA (buffer B_b). Immobilized Hrd1 liposomes or nanodiscs were ubiquitinated on the beads. Briefly, ubiquitination mix containing 0.2 µM Uba1, 2 µM Ubc7, 2 µM Cue1-c and 100 µM ubiquitin was prepared in buffer B_b. 20 µl ubiquitination mix was added per 20 µl beads. Ubiquitination was initiated by the addition of 2.5 mM ATP and performed at 30 °C for 1 h. In control experiments, ATP was omitted from the ubiquitination reaction. Beads were subsequently washed with buffer B_a. Substrates were diluted into freshly prepared buffer B_a immediately before use. This is critical as, in our experience, CPY* aggregates over time after dilution into urea-free buffer, resulting in reduced binding. The diluted substrates (final concentration: 20 nM) were incubated with 20 µl beads containing immobilized Hrd1 liposomes or nanodiscs for 30 min at room temperature. The supernatants were collected and the beads were washed with buffer B_a. The beads were eluted with 2 mM biotin in buffer B_a for 45 min at room temperature. For single-concentration binding experiments, the input, unbound and elution fractions were analysed by SDS–PAGE and fluorescence scanning in an Odyssey CLx scanner (Li-COR). For all titration experiments except PrA WT, the input and supernatants were pipetted into black 384-well plates with flat, transparent bottoms (Corning 3655) and the plate was scanned in an Odyssey CLx scanner. The fraction bound was determined by quantifying the unbound fraction and normalizing it to the unbound fraction in the beads-only control (fraction bound = 1 − unbound/unbound in beads only). For PrA WT, the quantification was performed in the same way, but from gels after SDS–PAGE and fluorescence scanning. Fitting was performed with Origin software using a one-site binding model assuming a 1:1 stoichiometry. The quantifications of substrate binding were from three independent experiments, with the exception of those in Fig. 3b,c, which were from four independent experiments. The error bars in the binding experiments indicate standard deviation.

Ubiquitin chain shortening binding assay. Ubiquitin chains on Hrd1 and Ubc6 were shortened by including K48R ubiquitin at specific ratios as a chain terminator during polyubiquitination on beads. Briefly, Hrd1 alone or Ubc6 and Cue1 were reconstituted into liposomes containing 2% biotinyl PE. After immobilization onto magnetic streptavidin beads, the ubiquitination mix was supplemented with a 1:8 ratio of K48R ubiquitin (Enzo Life Sciences) to WT ubiquitin (Boston Biochem) for medium chains and a 3:8 ratio of K48R ubiquitin to WT ubiquitin for short chains. No K48R ubiquitin was included for long chains. The ubiquitination mix for Ubc6/Cue1 liposomes contained 4 µM Doa10 RING domain and no Cue1-c. Ubiquitination was performed at 30 °C for 1 h, after which aliquots of liposomes were eluted from the beads with SDS sample buffer in +ATP and −ATP conditions to determine the degree of ubiquitination. Ubiquitination was performed on beads in a single batch and diluted into respective volumes of empty beads to ensure that the degree of ubiquitination was equal across all Ubc6 and Hrd1 concentrations. Following ubiquitination, the beads were washed with buffer B_a and CPY* binding experiments were carried out as described above. To determine the concentration of ubiquitinated Hrd1 or Ubc6 plotted on the *x* axis in Fig. 4b, the nominal concentrations were multiplied by the fraction of ubiquitinated Hrd1 or Ubc6.

Substrate release after deubiquitination. Hrd1 (250 nM) or Ubc6 and Cue1 (250 nM each) reconstituted into liposomes containing 2% biotinyl PE were immobilized onto magnetic streptavidin beads and ubiquitinated with WT ubiquitin to produce long chains. 20 µl of 50 nM CPY* in buffer B_a was added to 20 µl of beads. The beads were incubated with CPY* for 30 min at room temperature and the unbound fraction was collected. The beads were subsequently washed with buffer B_a and aliquots were eluted with SDS sample buffer to determine the total bound CPY*. 20 µl beads was incubated with 20 µl Usp2 (3 µM) in buffer B_a or 20 µl buffer B_a without Usp2. After incubation for 2 min at room temperature, the supernatant was collected (Usp2 Sup.) and the beads were subsequently eluted with SDS sample buffer to determine the fraction remaining on the beads. The samples were analysed by SDS–PAGE and fluorescence scanning with an Odyssey CLx scanner. The fraction of CPY* released was calculated by quantifying the amount of CPY* in the Usp2 Sup. and dividing this value by the total CPY* bound. Quantification was performed from three independent experiments. The centre values represent the mean and error bars indicate standard deviation.

Deubiquitination assay. Hrd1 liposomes (0.5 µM Hrd1 final concentration) were immobilized onto magnetic streptavidin beads and ubiquitinated for 1 h at 30 °C with ubiquitination mix, as described above. As a control, ATP was omitted from a set of reactions. The beads were washed after ubiquitination and eluted with 2 mM biotin. Increasing concentrations of Usp2 were incubated with the eluted Hrd1 liposomes and samples were pipetted into SDS sample buffer after 5 and 10 min. The samples were analysed by SDS–PAGE and fluorescence scanning with an Odyssey CLx scanner.

Anisotropy binding assay. Anisotropy measurements were performed at 25 °C in a Synergy 4 HT microplate reader (Biotek) in black 96-well half-area plates with a flat-bottom, non-binding surface (Corning 3686). Reactions were performed with 50 nM CPY* or 50 nM CPY WT, labelled with Alexa Fluor 488 (Thermo Fisher Scientific), in buffer containing 20 mM HEPES–KOH pH 7.4, 150 mM NaCl, 0.5 mM TCEP, 0.5 mg ml^{-1} BSA. Samples were mixed with the indicated amounts of Hrd1 nanodiscs or empty nanodiscs as a control. After incubation at 25 °C for 10 min, measurements were performed with the sensitivity set to 'auto'. Titrations with CPY* were repeated at least in triplicate ($n=5$ for −ATP and $n=4$ for +ATP). Titrations with CPY WT were repeated in triplicate. Experiments with empty nanodiscs were repeated twice.

Estimation of dissociation constant. To estimate the binding affinities for CPY* to non-ubiquitinated Hrd1 reconstituted in nanodiscs, the anisotropy changes or, for experiments with bead immobilization, the fraction of bound CPY* were first plotted against the total Hrd1 concentration. The data were then fitted assuming a stoichiometry of 1:1 according to the equation

$$y = y_{max} \times [\mathrm{Hrd1_{total}}]/(K_D + [\mathrm{Hrd1_{total}}])$$

As the concentration of CPY* was only 20 nM (for immobilized nanodiscs) or 50 nM (in the anisotropy experiment) for titrations with nanodiscs, which is well below the estimated dissociation constant, the difference between free Hrd1 and total Hrd1 was neglected. For immobilized Hrd1 nanodiscs, we estimated the apparent dissociation constant to be 126 ± 43 nM and for anisotropy titrations

450 ± 50 nM. For titration with ubiquitinated Hrd1 in nanodiscs, the affinity was markedly increased. However, the lack of sufficient data points in the lower concentration ranges meant that we could not reliably determine a dissociation constant.

Electron microscopy of nanodiscs. Samples were bound to a glow-discharged, carbon-foil-covered grid. After washing the grid with 5 µl 0.1% glutaraldehyde, the sample was stained with 1% uranyl acetate. Samples were evaluated using a Talos L120C transmission electron microscope equipped with a Ceta 16M camera (Thermo Fisher Scientific, FEI). The size distribution of the mean diameters of the structures was calculated using iTEM software (version 5.2) (Olympus Soft Imaging Solutions).

Statistics and reproducibility. All electrophysiological experiments were repeated in independent triplicates unless stated otherwise. The error bars of these experiments indicate the standard error. All statistical analysis of biochemical experiments was performed from a minimum of three independent experiments, with exact samples sizes stated in the figure legends. For biochemical experiments, the centre values represent the mean and error bars indicate standard deviation.

Reporting Summary. Further information on research design is available in the Nature Research Reporting Summary linked to this article.

Data availability

Source data for Figs. 1–4 and Extended Data Figs. 1–3 are provided with the paper. All other data supporting the findings of this study are available from the corresponding authors on reasonable request.

References

41. Popp, M. W. & Ploegh, H. L. Making and breaking peptide bonds: protein engineering using sortase. *Angew. Chem. Int. Ed. Engl.* **50**, 5024–5032 (2011).
42. Chen, I., Dorr, B. M. & Liu, D. R. A general strategy for the evolution of bond-forming enzymes using yeast display. *Proc. Natl Acad. Sci. USA* **108**, 11399–11404 (2011).
43. Hernandez, J. M. et al. Membrane fusion intermediates via directional and full assembly of the SNARE complex. *Science* **336**, 1581–1584 (2012).
44. Bello, O. D., Auclair, S. M., Rothman, J. E. & Krishnakumar, S. S. Using ApoE nanolipoprotein particles to analyze SNARE-induced fusion pores. *Langmuir* **32**, 3015–3023 (2016).
45. Harsman, A., Bartsch, P., Hemmis, B., Kruger, V. & Wagner, R. Exploring protein import pores of cellular organelles at the single molecule level using the planar lipid bilayer technique. *Eur. J. Cell Biol.* **90**, 721–730 (2011).
46. Denkert, N. et al. Cation selectivity of the presequence translocase channel Tim23 is crucial for efficient protein import. *eLife* **6**, e28324 (2017).
47. Reinhold, R. et al. The channel-forming Sym1 protein is transported by the TIM23 complex in a presequence-independent manner. *Mol. Cell. Biol.* **32**, 5009–5021 (2012).
48. Cohen, F. S., Niles, W. D. & Akabas, M. H. Fusion of phospholipid vesicles with a planar membrane depends on the membrane permeability of the solute used to create the osmotic pressure. *J. Gen. Physiol.* **93**, 201–210 (1989).
49. Smart, O. S., Breed, J., Smith, G. R. & Sansom, M. S. A novel method for structure-based prediction of ion channel conductance properties. *Biophys. J.* **72**, 1109–1126 (1997).
50. Hodgkin, A. L. & Katz, B. The effect of sodium ions on the electrical activity of giant axon of the squid. *J. Physiol.* **108**, 37–77 (1949).
51. Hotz, T. et al. Idealizing ion channel recordings by a jump segmentation multiresolution filter. *IEEE Trans. Nanobioscience* **12**, 376–386 (2013).

Acknowledgements

We thank O. D. Bello and J. E. Rothman for providing the construct for ApoE422K, I. Bickmeyer and N. Nupur for technical assistance and T. Rapoport and R. Jahn for comments on the manuscript. This work was supported by the European Research Council (ERC) under the Horizon2020 research and innovation programme (grant no. 677770) to A.S., by the Deutsche Forschungsgemeinschaft SFB1190, grant nos. P12 (to M.M.) and P15 (to A.S.), and a Boehringer Ingelheim Fonds PhD Fellowship (to V.V.).

Author contributions

A.S. and M.M. conceived the experiments and wrote the manuscript. V.V., N.D., D.R. and A.S. carried out the experiments: N.D. performed the electrophysiology; V.V. and A.S. performed the biochemistry; C.C.S. provided reagents and established the Ubc6-related experiments; and D.R. performed the electron microscopy. All authors contributed to data analysis.

Competing interests

The authors declare no competing interests.

Additional information

Extended data is available for this paper at https://doi.org/10.1038/s41556-020-0473-4.

Supplementary information is available for this paper at https://doi.org/10.1038/s41556-020-0473-4.

Correspondence and requests for materials should be addressed to A.S. or M.M.

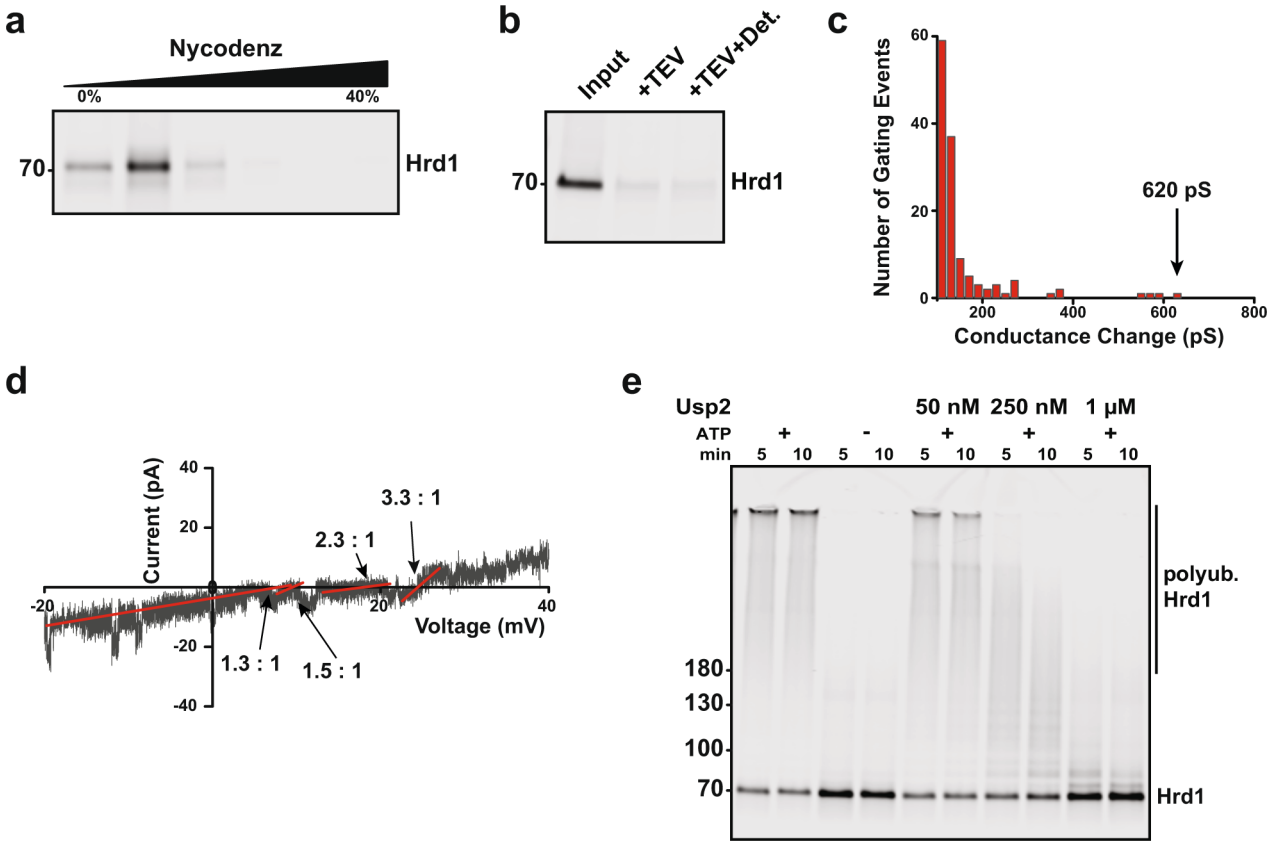

Extended Data Fig. 1 | Characterization of Hrd1 liposomes and channel properties. a, Liposomes containing C-terminally fluorescently labelled Hrd1 were floated in a Nycodenz step gradient. The gradient was fractionated and samples were analyzed by SDS-PAGE and fluorescence scanning. **b**, Fluorescently labeled Hrd1 in liposomes were incubated with Tobacco Etch Virus (TEV) protease that cleaves off the C-terminal SBP tag and the fluorescent dye. As a control, detergent-solubilized liposomes were incubated with TEV protease. Samples were analyzed by SDS PAGE and fluorescence scanning. **c**, Conductance state histogram zoom plot of Fig. 1e. The arrow and number indicate the highest observed conductance state for ubiquitinated Hrd1. To focus on large conductance states, the zoom plot starts at 100 pS. **d**, Current-voltage relationship of ubiquitinated Hrd1 at asymmetric salt. Arrows indicate the various reversal potentials and the numbers give the corresponding relative selectivities of potassium over chloride as calculated from the Goldman-Hodgkin-Katz equation. The red line represents linear regression (least-squares) of indicated data regions (length of red line on x-axis). Shown is a representative trace of three independent experiments. **e**, Time course of deubiquitination of Hrd1 using indicated concentrations of Usp2. Liposomes containing fluorescently labeled Hrd1 were immobilized onto streptavidin magnetic beads and incubated with ubiquitination mix in the presence or absence of ATP. After washing, Hrd1 liposomes were eluted with 2 mM biotin and incubated with the indicated amount of Usp2. The reaction was stopped by addition of SDS sample buffer. Samples were analyzed by SDS-PAGE and fluorescence scanning. This particular experiment was performed once. Other related deubiquitination experiments are shown in Fig. 3a and Extended Data Fig. 3a. In **a-b**, representative images of three independent experiments are shown. Source data and unprocessed gels are provided in Source Data Extended Data Fig. 1.

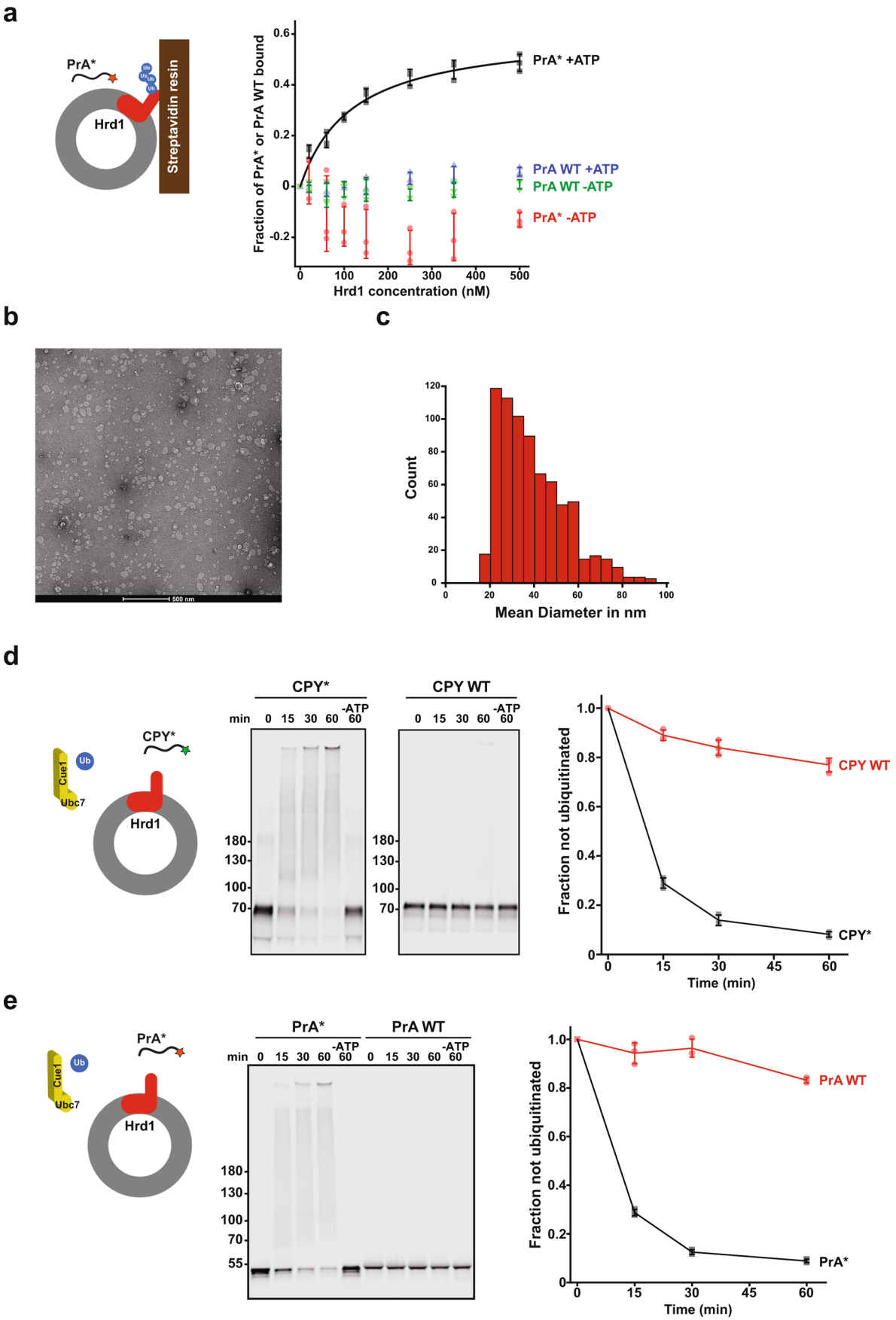

Extended Data Fig. 2 | See next page for caption.

Extended Data Fig. 2 | Interaction of misfolded substrates with Hrd1 reconstituted in liposomes or nanodiscs. a, PrA*, but not PrA WT interacts with ubiquitinated Hrd1. Indicated amounts of Hrd1 liposomes were immobilized onto streptavidin magnetic beads via the C-terminal SBP tag on Hrd1. After incubation with ubiquitination mix in the presence or absence of ATP, beads were washed and incubated with 20 nM PrA* or 20 nM PrA WT at the indicated Hrd1 concentrations. The fraction of bound PrA* or PrA WT was determined from the supernatants. mean ± s.d (n = 3 independent experiments). **b**, Negative stain electron micrographs of glutaraldehyde-fixed Hrd1 nanodiscs. **c**, Size distribution from n = 738 Hrd1 nanodiscs. **d**, CPY*, but not CPY WT is efficiently ubiquitinated when added to the outside of Hrd1 in liposomes. Left: Fluorescently labelled CPY* or CPY WT (100 nM) was added to liposomes containing Hrd1 (200 nM) and incubated with ubiquitination mix with or without ATP. Samples from indicated time points were analyzed by SDS-PAGE and fluorescence scanning. Right: Quantification of three ubiquitination experiments. These data are also presented in Fig. 3h (CPY* lipos) and Extended Data Fig. 3c, d (CPY WT, WT Hrd1). mean ± s.d (n = 3 independent experiments). **e**, PrA*, but not PrA WT is efficiently ubiquitinated when added to the outside of Hrd1 in liposomes. Left: Fluorescently labelled PrA* or PrA WT (100 nM) was added to liposomes containing Hrd1 (200 nM) and incubated with ubiquitination mix with or without ATP. Samples from indicated time points were analyzed by SDS-PAGE and fluorescence scanning. Right: Quantification of three ubiquitination experiments. mean ± s.d (n = 3 independent experiments). Source data and unprocessed gels are provided in Source Data Extended Data Fig. 2.

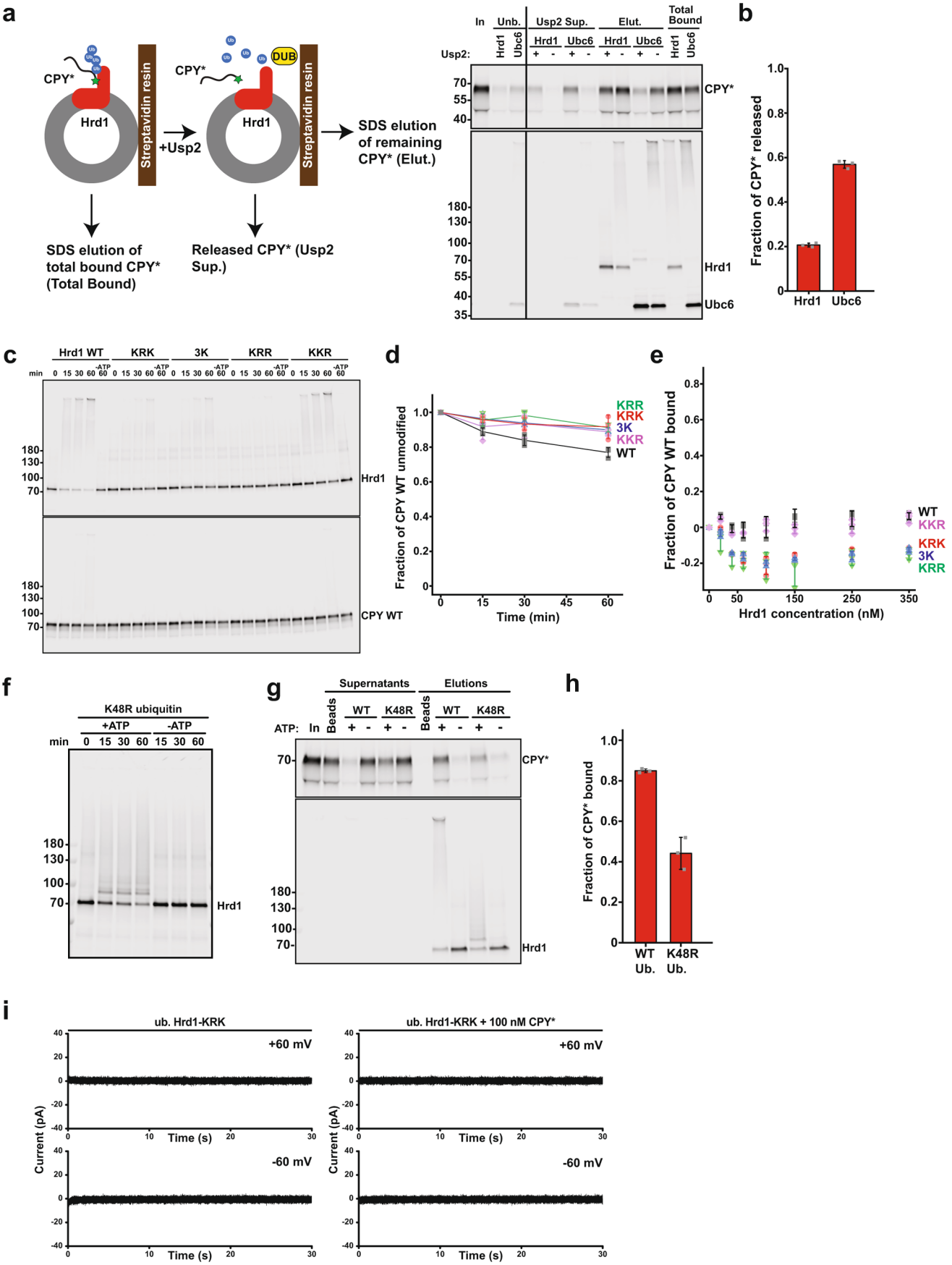

Extended Data Fig. 3 | See next page for caption.

Extended Data Fig. 3 | Characterization of the interaction of CPY* with autoubiquitinated Hrd1. a, Release of CPY* from liposomes containing ubiquitinated Ubc6 or Hrd1 upon deubiquitination. Beads with immobilized liposomes containing ubiquitinated Hrd1 (250 nM) or ubiquitinated Ubc6 (250 nM) were incubated with CPY* (50 nM). After washing, an aliquot of beads were incubated with SDS sample buffer to determine the total bound CPY*. Usp2 (3 μM) was added to the beads and the supernatant was collected. The Usp2 treated samples were then eluted with SDS sample buffer. Samples were analyzed by SDS PAGE and fluorescence scanning. In: CPY* input to the beads, Unb: unbound CPY* after incubation with ubiquitinated Hrd1 or Ubc6. **b**, Quantification (mean ± s.d.) of the fraction of CPY* released upon deubiquitination by Usp2 from three experiments as in **a**. **c**, CPY WT (100 nM) was incubated with fluorescently labeled WT Hrd1 or indicated mutants in liposomes (200 nM), and ubiquitination mix with or without ATP. Samples from indicated time points were analyzed by SDS-PAGE and fluorescence scanning. **d**, Quantification (mean ± s.d.) of three experiments as in **c**. **e**, Increasing concentrations of ubiquitinated, bead-immobilized WT Hrd1 or indicated Hrd1 mutants in liposomes were incubated with fluorescently labeled CPY WT (20 nM). The bound fraction was quantified from supernatants. mean ± s.d (n = 3 independent experiments). **f**, Liposomes containing fluorescently labeled Hrd1 were incubated with ubiquitination mix containing the ubiquitin K48R mutant. Samples were analyzed by SDS PAGE and fluorescence scanning. Shown is a representative image of two independent experiments. **g**, Bead-immobilized Hrd1 liposomes were incubated with ubiquitination mix containing WT or K48R ubiquitin with or without ATP. Beads were then subsequently incubated with fluorescently labelled CPY* (40 nM). Samples were analyzed by SDS PAGE and fluorescence scanning. **h**, Quantification (mean ± s.d.) of three experiments as in **g**. **i**, Constant-voltage recordings of ubiquitinated Hrd1 KRK mutant at indicated voltages in the absence (left) and presence of CPY* (right). Shown are representative traces of three independent experiments. Source data and unprocessed gels are provided in Source Data Extended Data Fig. 3.

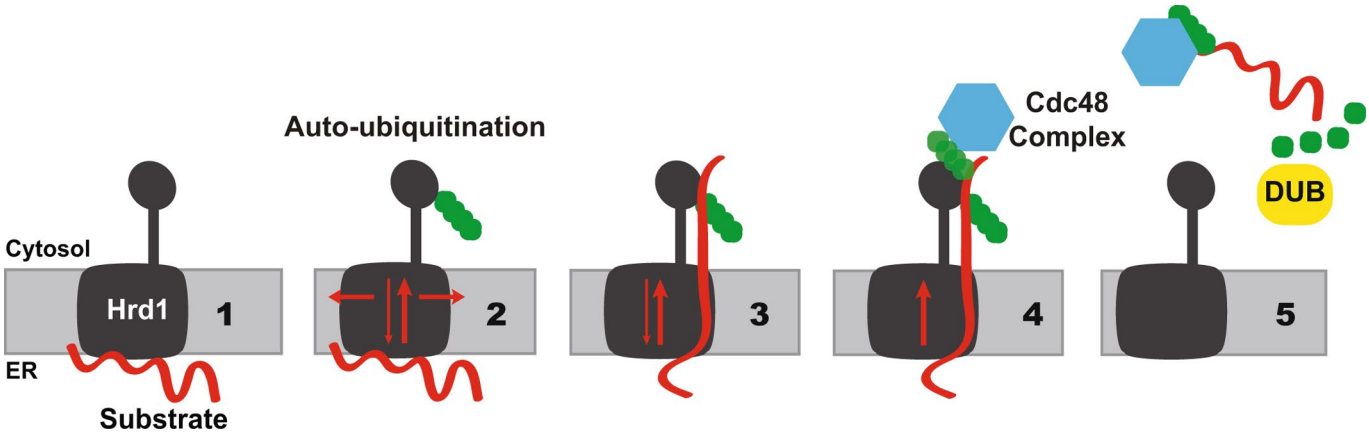

Extended Data Fig. 4 | Molecular mechanism for Hrd1-dependent retrotranslocation of misfolded proteins from the ER lumen to the cytosol. A Misfolded substrate binds to the luminal face of Hrd1 (**1**). Hrd1 auto-ubiquitination opens the retrotranslocation pore (**2**) which is further expanded by substrate insertion. A high-affinity binding site on the cytoplasmic face of Hrd1 drives initial substrate translocation (**3**). The substrate is ubiquitinated by Hrd1 on the cytoplasmic side of the membrane and recruits the Cdc48 complex (**4**). The Cdc48 complex segregates substrate and Hrd1, and extracts the ubiquitinated substrate from the membrane through rounds of ATP hydrolysis. Hrd1 is deubiquitinated by a DUB, closing the retrotranslocation pore (**5**).

nature research

Corresponding author(s): Michael Meinecke & Alexander Stein

Last updated by author(s): Jan 9, 2020

Reporting Summary

Nature Research wishes to improve the reproducibility of the work that we publish. This form provides structure for consistency and transparency in reporting. For further information on Nature Research policies, see Authors & Referees and the Editorial Policy Checklist.

Statistics

For all statistical analyses, confirm that the following items are present in the figure legend, table legend, main text, or Methods section.

n/a	Confirmed	
☐	☒	The exact sample size (*n*) for each experimental group/condition, given as a discrete number and unit of measurement
☐	☒	A statement on whether measurements were taken from distinct samples or whether the same sample was measured repeatedly
☒	☐	The statistical test(s) used AND whether they are one- or two-sided *Only common tests should be described solely by name; describe more complex techniques in the Methods section.*
☒	☐	A description of all covariates tested
☐	☒	A description of any assumptions or corrections, such as tests of normality and adjustment for multiple comparisons
☐	☒	A full description of the statistical parameters including central tendency (e.g. means) or other basic estimates (e.g. regression coefficient) AND variation (e.g. standard deviation) or associated estimates of uncertainty (e.g. confidence intervals)
☒	☐	For null hypothesis testing, the test statistic (e.g. *F*, *t*, *r*) with confidence intervals, effect sizes, degrees of freedom and *P* value noted *Give P values as exact values whenever suitable.*
☒	☐	For Bayesian analysis, information on the choice of priors and Markov chain Monte Carlo settings
☒	☐	For hierarchical and complex designs, identification of the appropriate level for tests and full reporting of outcomes
☒	☐	Estimates of effect sizes (e.g. Cohen's *d*, Pearson's *r*), indicating how they were calculated

Our web collection on statistics for biologists contains articles on many of the points above.

Software and code

Policy information about availability of computer code

Data collection	Axoscope 10.3 (Molecular Devices), Clampex 10.3 (Molecular Devices), iTEM (Olympus), Image Studio (Li-COR)
Data analysis	Microsoft Excel, Image Studio (Li-COR), Origin (OriginLab), R (stepR package), iTEM (Olympus)

For manuscripts utilizing custom algorithms or software that are central to the research but not yet described in published literature, software must be made available to editors/reviewers. We strongly encourage code deposition in a community repository (e.g. GitHub). See the Nature Research guidelines for submitting code & software for further information.

Data

Policy information about availability of data

All manuscripts must include a data availability statement. This statement should provide the following information, where applicable:

- Accession codes, unique identifiers, or web links for publicly available datasets
- A list of figures that have associated raw data
- A description of any restrictions on data availability

Source data for statistical analysis as well as unprocessed gels for all figures are provided online. All other data supporting the findings of this study are available from the corresponding authors on reasonable request.

Field-specific reporting

Please select the one below that is the best fit for your research. If you are not sure, read the appropriate sections before making your selection.

☒ Life sciences ☐ Behavioural & social sciences ☐ Ecological, evolutionary & environmental sciences

For a reference copy of the document with all sections, see nature.com/documents/nr-reporting-summary-flat.pdf

Life sciences study design

All studies must disclose on these points even when the disclosure is negative.

Sample size	No sample-size calculations were performed. Instead, the sample sizes were based on the magnitude or consistency of differences between the tested conditions/groups. We found that for most of experiments, sample sizes of n=3 led to conclusive and compelling results.
Data exclusions	No data was excluded
Replication	To ensure reproducibility of the study, all quantitative experiments were repeated at least three times (exact numbers for each experiment are stated in the manuscript), except Fig. 3f, where one condition was repeated twice. All attempts at replication were successful.
Randomization	Randomization was not applicable in any of the experiments. The experiments in this study were almost exclusively quantitative and the data were acquired by machines. Therefore, experimenter bias was not relevant.
Blinding	As described above, experimenter bias was not relevant to this study due to its quantitative and technical nature. Therefore, we did not find blinding to be necessary.

Reporting for specific materials, systems and methods

We require information from authors about some types of materials, experimental systems and methods used in many studies. Here, indicate whether each material, system or method listed is relevant to your study. If you are not sure if a list item applies to your research, read the appropriate section before selecting a response.

Materials & experimental systems

n/a	Involved in the study
☒	☐ Antibodies
☐	☒ Eukaryotic cell lines
☒	☐ Palaeontology
☒	☐ Animals and other organisms
☒	☐ Human research participants
☒	☐ Clinical data

Methods

n/a	Involved in the study
☒	☐ ChIP-seq
☒	☐ Flow cytometry
☒	☐ MRI-based neuroimaging

Eukaryotic cell lines

Policy information about cell lines

Cell line source(s)	Saccharomyces cerevisiae: BY4741, BY4742 (Open Biosystems), InvSc1 (Invitrogen)
Authentication	Saccharomyces cerevisiae was used for protein expression only. Chromosomal deletion strains were validated by PCR genotyping. Strains containing expression plasmids were selected with auxotrophic markers.
Mycoplasma contamination	Cell lines were not tested for mycoplasma contamination. This is not normally done for S. cerevisae strains.
Commonly misidentified lines (See ICLAC register)	No commonly misidentified cell lines were used in this study.